Review

Jaroslaw Mysliwiec*, Alina Szukalska, Adam Szukalski and Lech Sznitko

Liquid crystal lasers: the last decade and the future

https://doi.org/10.1515/nanoph-2021-0096
Received March 8, 2021; accepted April 21, 2021;
published online June 4, 2021

Abstract: The demonstration of the first ruby laser in 1960 led to a revolution in science and technology. The lasers have significantly influenced the development of new approaches to spectroscopy, giving previously undreamed insights into physics, chemistry, and other scientific areas. The search for new materials for light amplification is one of the fundamental subjects of modern photonics and nanotechnology. In this review, we summarize the most appealing progress in developing liquid crystalline (LC) micro and nano-lasers during the last decade, together with their applications and description of perspectives for the future. We will describe the physical background necessary to understand the operation principles of LC lasers, including a description of radiative transition phenomena and LC matter. The article will be divided into separate sections concerning different approaches of LC lasers realization, including; band edge, DFB, DBR, VECSEL, and random cavities utilization. We will also discuss how the LC phases can influence the design of laser devices. Finally, the potential applications, perspectives, and conclusions will be discussed at the end of the article.

Keywords: blue phase; microlasing; nanolasing; plasmonic lasers; random lasing.

1 Introduction

Liquid crystals (LCs) belong to the soft matter class that merges the properties typical of crystals and liquids. A combination of fluidity and long-range orientational order enables easy tuning of their properties affected by optical, magnetic, and electric fields. Goldberg, and Schnur put forward the original concept of lasing in liquid crystal laser in 1973 [1], but the first experimental demonstration was done 25 years later by Kopp et al. [2] Since then, multiple studies have addressed the utilization of LCs in light amplification phenomena [3, 4]. Mirrorless lasing was observed in one-dimensional helical cholesteric materials [5], three-dimensional photonic-bandgap materials [6], free-standing cholesteric liquid single crystal elastomers [7], or chiral ferroelectric smectic materials [8]. Various methods of emission tuning were also developed and presented [9–15]. Despite the passage of so many years, liquid crystalline systems still have attracted considerable attention because of their potential application in devices devoted to controlling light propagation. These materials can slow down and even trap light with frequencies in close vicinity of the photonic band-gap. Therefore, such materials are interesting for applications in designing new laser light sources. Tunable resonators or lasers, including distributed feedback (DFB), distributed Bragg reflectors (DBRs), or in the form of vertical-cavity emitters [called vertical-cavity surface-emitting lasers (VCSELs)] can tune the resonance frequency through changes in size, shape, or temperature or the external electric field. Nonclassic laser action can be obtained either in systems with gain or refractive index (periodic) distribution pumped by a suitable light source, inducing population inversion or random light scattering in amplifying medium containing luminescent dye. The latter mentioned process is called random lasing, which was achieved in various LC-based media, like luminescent organic dye, semiconductor, or perovskite-doped nematics and polymer-dispersed LCs (PDLCs). Other investigated constructions include microlasers in the form of whispering gallery mode (WGM) based systems (plasmonic and biological).

In this comprehensive review, we try to summarize the most appealing progress in developing liquid crystalline micro and nano lasers during the last decade, together with their applications and description of perspectives for the future.

***Corresponding author: Jaroslaw Mysliwiec**, The Advanced Materials Engineering and Modelling Group, Wroclaw University of Science and Technology, Wyb. Wyspianskiego 27, 50-370, Wroclaw, Poland, E-mail: jaroslaw.mysliwiec@pwr.edu.pl. https://orcid.org/0000-0002-1244-9863
Alina Szukalska, Adam Szukalski and Lech Sznitko, The Advanced Materials Engineering and Modelling Group, Wroclaw University of Science and Technology, Wyb. Wyspianskiego 27, 50-370, Wroclaw, Poland

2 Light amplification

The light amplification can be obtained in optical systems as a result of stimulated emission (STE) [16] or through the nonlinear optical (NLO) processes [17]. The first-mentioned case is requiring the population inversion state to make STE be more probable than spontaneous emission. For such conditions, more molecules/atoms are in the excited state, and the process of photon absorption is less probable than the STE occurrence. When a photon approaches a matter and if its' energy is equal to the size of the energy gap between the ground and excited state, once it can be absorbed or can trigger the radiative transition through the STE. In the latter case, an incident photon is "copied," an identical photon is generated, and thus the intensity of output light is increased. The generated quant of radiative energy in STE has the same energy, phase, polarization, and propagation direction as the photon triggering the transition. In the medium, in population inversion state and length L, the light intensity is growing exponentially relative to the traveled distance. This process is similar to the *Lambert-Beer* law of absorption; however, with a negative absorption coefficient γ [18, 19] called net gain coefficient:

$$I(L) = I_0 e^{\gamma L} = I_0 e^{(g-\alpha)L}, \tag{1}$$

where $I(L)$ – is the intensity of the output beam, and I_0 – is the intensity of incident light.

A comparison of the absorption and STE is shown on energetic diagrams presented in Figure 1(a) and (b), respectively. A schematic representation of light amplification in the STE process is shown in Figure 1(c). In Figure 1(d), one can compare the rate of light intensity increase during the propagation in gain media characterized by different net gain coefficients.

The population inversion cannot be sustained without external pumping. The energy must be delivered to the gain medium so that the material can provide gain. The most popular pumping methods are (*i*) optical pumping – where an external light source, like flash-lamps or other lasers, are utilized to deliver the energy to the gain medium; (*ii*) electric pumping – where electric charge provides the energy to the gain media, for example, as glow discharge in gases or as the holes and electrons recombination in semiconducting material [16]. More unusual energy delivery methods are also possible, including chemical reactions, adiabatic cooling of gas during the supersonic flow, or even nuclear fission [16, 20, 21]. However, the exceptionally high pumping rate is not always sufficient to sustain the population inversion state. For example, the gain media has to be characterized by specific arrangements of electronic and vibrational energy levels with particular life-times [16, 18, 19]. Also, in stationary conditions, a two-level system cannot reach a state of population inversion. Therefore, additional energy levels must be involved to provide efficient pumping.

Different types of energetic systems are discussed in the literature, but the most important are three- and four-level systems. The first one is utilizing an intermediate $T1$ metastable state to obtain population inversion with respect to the ground state G. The excited state $S1$ is used

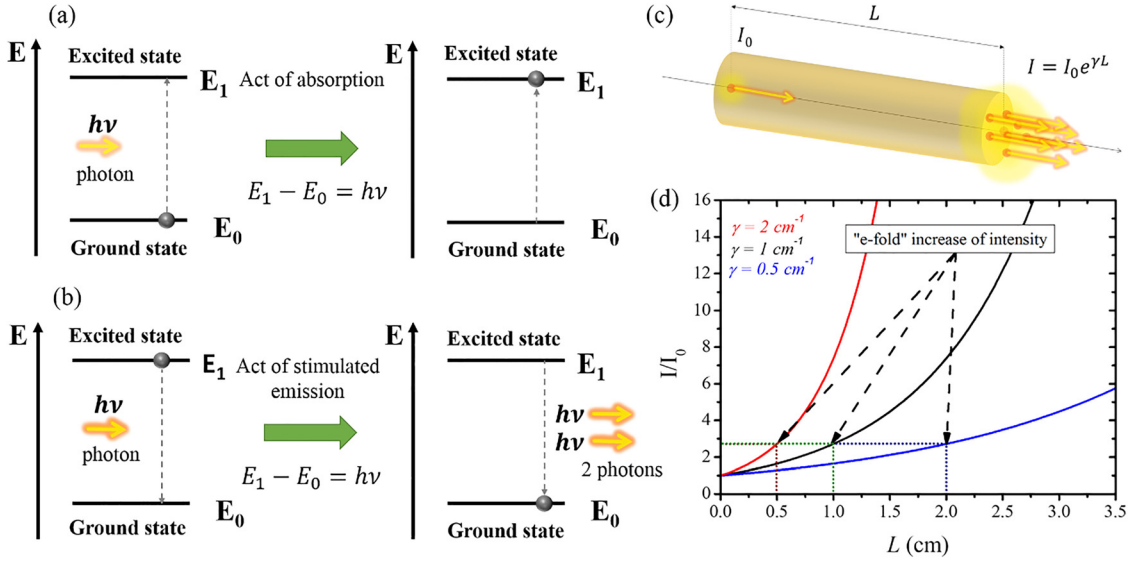

Figure 1: Scheme of absorption (a) and STE (b) processes depicted in energy diagrams. A scheme of amplification of light propagating through the gain medium (c). Different rates of intensity increase regarding different gain coefficients γ: 0.5, 1, and 2 cm^{-1} (d).

only to provide energy to the system from a pumping source (see Figure 2(a)). A three-level system was utilized to obtain the laser emission in the first laser – the ruby laser [22]. Laser materials showing this type of energetic level layout are affected by relatively high thresholds of laser action. The four-level systems are much more advantageous. In that case, an additional state $S1$ is placed slightly above the ground state $S0$. The highest $S3$ state is pumped directly from the state $S0$; then, rapid relaxation occurs to the $S2$ positioned slightly below the $S3$. The $S2$ to $S1$ transition is a radiative one, with the emission of a photon. The relaxation from $S1$ to $S0$ is very fast, usually when the energy difference between $S1$ and $S0$ states is small. Therefore, the $S2$ is always in a population inversion state to the $S1$ level (see Figure 2(b)), and the light amplification is easily achievable. The schematic comparison between the three-level and four-level systems is shown in Figure 2(a) and (b), respectively.

The amplification of light is also achievable using nonlinear optical processes. Those effects can be applied to light amplification using two different approaches. In the first case, called parametric amplification, the light is amplified in the process of difference-frequency generation [17]. The pumping light of frequency ν_p is transforming the matter from ground state G into the virtual state VS2. Next, the relaxation to another virtual state VS1 is accompanied by the generation of photons of frequency ν_S called a signal photon. Note that $\nu_S < \nu_p$. Additional energy is also emitted in the form of quant of radiative energy of frequency ν_i called idler photon and the system relaxes to the ground state G. Thus, the sum of signal and idler frequency is equal to pumping frequency according to the relation: $\nu_P = \nu_S + \nu_i$, therefore the process is parametric. If the matter is in virtual state VS2 and the signal photon is incident, it can trigger identical photons' emission in the same manner as it is for STE. The difference is that the emission is occurring from one virtual stage to another virtual state. The rest of the amplification process is analogical to the STE. A schematic diagram of transitions during parametric amplification is depicted in Figure 3(a). The optical devices capable of amplifying the light in parametric amplification are called optical parametric amplifiers (OPA) [23]. Next to these devices, one can distinguish so-called optical parametric oscillators (OPO), which utilizes a cavity to provide the feedback mechanism [23].

The parametric amplification is related to the second-order nonlinear optical susceptibility $\chi^{(2)}$, which requires noncentrosymmetric nonlinear-optical media, and thus the number of suitable materials for this purpose is limited. Some efforts have been made to develop nonlinear amplifiers using third-order NLO processes (proportional to $\chi^{(3)}$) [24]; they can have a centrosymmetric structure. However, lower magnitudes of higher-order nonlinearities require longer distances, and those devices are mainly designed in the form of NLO fibers.

The second approach is utilizing the effect of Two-Beam Coupling (TBC) in NLO material. The NLO media must exhibit the ability to change the refractive index value upon the influence of incident light. As shown in Figure 3(b), two coherent beams interfere in such NLO material. In that case, the interference pattern in the form of sinusoidal intensity distribution will be reflected in the

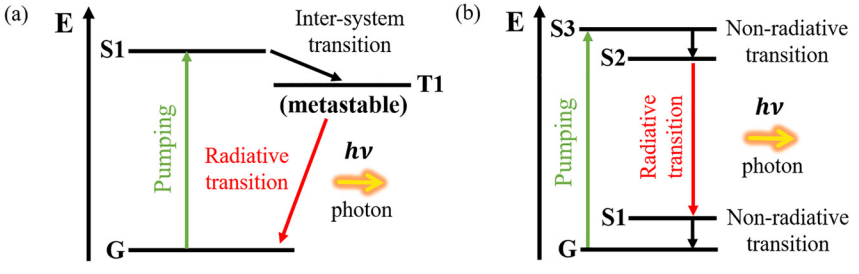

Figure 2: Comparison of three- (a) and four- (b) level systems used for the light amplification process.

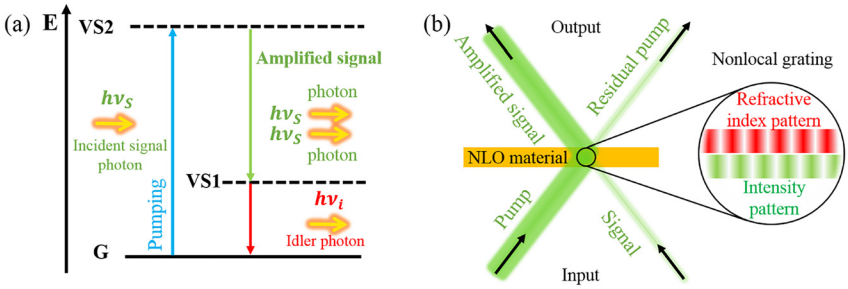

Figure 3: Nonlinear parametric amplification (a) and holographic amplification of light in TBC configuration (b).

material's refractive index spatial distribution. In other words, the interfering light will generate the phase grating inside the NLO media. Quite a common phenomenon observed for light-induced gratings is the nonlocality of induced gratings [25]. Nonlocality means that the refractive index pattern is phase-shifted relative to the intensity's sinusoidal distribution in the interference pattern. This shift is responsible for symmetry breaking, and thus, the intensity of light self-diffracted on the nonlocal grating is also asymmetric. This effect is schematically presented in Figure 3(b). Two interfering beams, pump, and signal are generating the nonlocal grating in photorefractive material. The pumping beam has a higher intensity than the signal beam. One could expect that pumping light diffracted into zero order of diffraction should also have a higher intensity than the signal beam diffracted into zero order of diffraction. However, due to the symmetry breaking, more light is diffracted into the direction of signal beam propagation. Thus, the zero-order of the signal beam is amplified by the cost of pumping beam energy. The signal beam can be efficiently amplified in proper conditions to reach the gain coefficient in the range of a few to tens of thousands of inverse centimeters for photorefractive liquid crystalline systems [26, 27]. The effect of beam coupling requires the material to exhibit the photorefractive phenomena; thus, it is strictly related to 3-rd order nonlinearities characterized by $\chi^{(3)}$ tensor.

2.1 Lasers – principles of operation

The LASER acronym can be expanded as light amplification by stimulated emission of radiation. Therefore, all lasers will utilize the STE phenomenon to obtain light amplification (see paragraph (a) in Section 2.1). Here, it should be noted that the acronym, as mentioned above, is specifically useful for a class of devices representing the self-excited amplifiers. Frequently, lasers are also called light generators. This is because they generate, filtrate, and amplify the optical signal. Thus, they require a feedback mechanism to operate. Optical amplifiers are another class of devices crucial for STE. Those types of devices use an optical medium sustained in the population inversion state to provide light amplification. However, they do not utilize the feedback mechanism, and thus, they are not considered lasers. Erbium amplifiers are devices that use STE for light amplification but not generation. They are frequently used in telecommunication to restore the optical signal after losses experienced during the propagation at long distances in optical fibers [28]. The difference between lasers and optical amplifiers is similar to the difference between OPO and OPA; however, in this case, STE plays the leading role in gain delivery. The first laser – the ruby laser, was constructed in 1960 by Theodore Maiman [22]. Since then, many types and classes of lasers have been built, including gas, dye, and semiconductor lasers. The typical laser consists of three main parts: the gain medium, the pump, and the optical cavity:

2.1.1 Gain medium

The gain medium is an optical material responsible for light amplification. The gain medium provides the optical gain (Eq. (1)) through the phenomenon of STE (see Section 2.1 (a)). The spectral properties of gain media determine the laser device's emission parameters, including the wavelength of emission, output intensity, and operation type (continuous wave or pulsed). The part of the electromagnetic field spectra responsible for light enhancement is called the gain profile because it determines what spectral width within the light amplification is achievable. Each gain material has its characteristic gain profile. Depending on assumed lasing parameters, the proper gain media must be selected for further laser device construction and application. Among the many types of laser materials, representing different states of matter, including gases, solid states, and liquids, one can distinguish: He–Ne, He–Cd gasses, Ar^+ or Kr^+ ionized gasses, rare-earth ions-doped crystals (e.g., Nd:YAG and Nd:YLF), and ion-doped crystals [e.g., Ruby (Cr^{3+} ions in Al_2O_3 matrix) and Ti:Sapphire (Ti^{3+} ions in Al_2O_3 matrix)], semiconducting inorganic diodes (e.g., AlGaAs or GaN), organic semiconducting polymers [e.g., MEH-PPV or polyfluorene (PF)], liquid organic dye solutions (e.g., xanthene or coumarin-type dyes), and many more [16, 18, 19, 29].

2.1.2 Pump

The pump is the device or physical/chemical process responsible for delivering energy necessary to keep the gain media in a population inversion state. There are many types of pumping processes. The most popular is optical pumping – where an external light source is used to excite the gain media through photon absorption. For this purpose, arc lamps, flash lamps, and other lasers can be used. Another type of electric pumping is where an electric charge is used to deliver the energy to sustain the gain media in the population inversion state. That could be the electric discharge in gas environments or the recombination of holes and electrons in semiconducting devices. Less famous but utilized in the construction of high-power lasers are chemical reactions, generating a vast amount of

vibrational energy or even nuclear reactions, producing a massive amount of high-energy charged particles interacting with gain media in the form of gasses or aerosols [16, 20, 21].

2.1.3 Feedback loop

The optical element of laser construction is responsible for multiplex amplification of light passing through the laser material; it determines the polarization and direction of light propagation and is responsible for selecting wavelengths from the available gain profile. The feedback is also increasing the energy density of radiative energy, allowing the STE to occur with higher probability and, thus, a lower threshold (relative to the lack of feedback) [16, 18, 19, 29]. Optical feedback could be realized in optical elements called cavities, frequently called resonators. Most of these are realizing the coherent feedback loops, for which the optical wave passing through the gain media is amplified through the addition of amplitudes of the generated part of electromagnetic waves. Thus, the influence of the phase of light is crucial for this kind of feedback mechanism. The other type, called incoherent feedback, is based on the addition of optical signals that are not coherent with each other. Thus, the amplification is based only on the intensity addition.

Typically, most laser resonators realize the coherent feedback mechanism and are in the form of cavities of different types and shapes. The most important types of resonators are the following:

(*i*) The *Fabry–Perot (F–P) resonator* consists of two mirrors facing each other with the gain medium between them. One of the mirrors, called the output coupler, is partially transparent and is used as the "window" to extract the laser light outside the cavity. The generated light is multiply reflected and forms the standing wave (longitudinal mode) inside the cavity; thus, the particular wavelengths, depending on cavity size, are selected according to the equation [16].

(*ii*) *Distributed feedback (DFB) resonators:* This kind of cavity was one of the first attempts to miniaturize lasers and provide a more compact design. Shank and Kogelnik first proposed this idea in the early 1970s [30]. The DFB resonators are formed as gain media with spatially occurring periodical changes of the refractive index, gain coefficient, or both at the same time. In the first case, the gain medium serves as one (or more) dimensional photonic crystal, where periodic modulation of the refractive index produces the photonic stop band positioned at the wavelength given by Bragg conditions [16, 19, 29]: $m\frac{\lambda}{2} = n_{\text{eff}}\,\Lambda$, where: m is an order of light diffraction, n_{eff} is an effective refractive index value, and Λ is the period of refractive index spatial modulation. The Bragg frequency is forbidden in the stop-band; no light of this frequency (wavelength) can exist in the photonic structure. However, in close vicinity of the photonic stop-band, so-called band edges, photons can propagate with group velocity nearly equal to zero. Very long persistence time of photons results in the light experiencing very high gain, and thus the band-edge lasing can be established. The laser emission in such conditions can occur in two modes surrounding the Bragg frequency. If the periodic modulation refers to the gain coefficient, there is no stop-band in the frequency domain. Thus, the light is precisely emitted at the Bragg frequency to obtain single-mode operation [16, 19, 29].

(*iii*) *Distributed Bragg-Reflector (DBR)*: this type of cavity uses the so-called Bragg reflectors (BRs) placed at least at one end of the gain medium [16, 19, 29]. The BRs are mirrors consisting of periodically arranged areas of high and low refractive indices. Similar to the DFB structure, such mirrors have a stop-band for a particular frequency. They provide selective light reflection (for particular Bragg frequency) with a very high reflectance parameter, much higher than regular reflectors. The BR can be integrated directly into the gain media, quite similar to DFB lasers, or placed outside for *F–P* resonators. The high reflectance makes DBR resonators very effective; thus, they are suitable for fabrications microsized lasers devices. The lasing wavelength conditions are similar to the *F–P* cavity because the cavity's length determines the lasing wavelength. Nevertheless, the periodic structure must be optimized for the mentioned wavelength of laser operation.

(*iv*) *Whispering Gallery Mode (WGM) cavity:* These cavities use the round shape of the gain medium, characterized by a refractive index value higher than for the surrounding environment. In such conditions, the total internal reflection can cause light localization in the gain medium. The light is "sliding" on the gain media perimeter's surface, allowing the interference to form the so-called WGMs. Due to the cavity's round shape, the light can travel very long paths inside the WGM resonator, even if it is very small. Therefore, the light inside such a cavity can experience very high amplification and, thus, lasing can be obtained in structures of micrometer-scale sizes. Moreover, the emission from WGM cavities is not unidirectional. However, their emission's directionality depends on the size of the cavity and light's polarization [19, 29, 31].

(v) *Random cavity (RC):* This type of resonator uses the effect of multiple light scattering to provide feedback. In general, light scattering in gain media is responsible for optical losses, negatively influencing the lasing properties. However, when scattering is strong enough to force photons to follow a diffusion-like propagation, the persistence time in gain media is rising. Thus, the light is experiencing a much higher gain compared to the ballistic propagation of photons. The light diffusion in 3D supports, as mentioned above, the incoherent feedback mechanism, making random lasers quite different from classical lasers with coherent feedback. A random laser (RL) emission can be omnidirectional, characterized by a broad lasing spectrum retrieving the gain profile. In that sense, the RL phenomenon can be similar to the amplified spontaneous emission (ASE). However, by the presence of positive feedback, the amplification is much higher in the RL case. Extreme scattering in complex media can also lead to light localization effects, and thus, the feedback mechanism is coherent because the influence of light interference cannot be neglected. In such a case, the RL is similar to a classic laser operation. However, the sharp lasing modes are randomly appearing in the spectrum [32].

3 Liquid crystals and lasers: why are they consistent?

LCs represent the state of matter that owns the ability to flow – just like liquids, and is characterized by long-range order – typical for crystals. Flowing ability makes LCs suitable for external control by electric or magnetic fields and mechanical forces [33]. On the other hand, the molecular order is responsible for the high anisotropy of physical properties that they can exhibit. For instance, the LCs show a high value of optical birefringence, typically around $\Delta n \approx 0.1$. However, using a smart molecular design allows obtaining LC mixtures with extremely high values, oscillating around $\Delta n \approx 0.7 - 0.8$ [34].

Most liquid crystalline materials commonly utilized in the industry are composed of rod-like molecules; however, banana or disc-shaped molecules are also known to form liquid crystalline phases [33, 35]. Most of the already known liquid crystalline materials represent the group of thermotropic LCs. In such a case, the occurrence of mesophase is determined by a specific range of temperatures. Above this range, the substance is melting to liquid form, and below, it solidifies. Next to thermotropic phases, one can distinguish lyotropic LCs, where the phase occurrence is determined by a specific concentration of a mesogen in a solution. Another type is phototropic LCs, for which the occurrence of mesophase is determined by the illumination of an external light source. In this case, the photo-transformation process is necessary to create the proper amount of conformers capable of generating liquid crystallinity [36]. Both latter phases play a rather marginal role in the industry, while rod-like thermotropic LCs are widely utilized in display applications.

As mentioned above, LCs are exhibiting the ordering of molecules. The molecules composing the mixture are aligned in different manners relative to other molecules depending on the mesophase type. To understand how different mesophases are defined, the following concepts must be explained:

(i) **Director *n***, the unit vector indicating rod-like molecules' orientation in a certain point of liquid crystalline phase, it also represents the local optical axis since rod-like molecules are forming uniaxial optical crystals [33].

(ii) **Scalar order parameter *S***, the value defined as [37]:

$$S = \frac{1}{2}\langle 3\cos^2\beta - 1\rangle, \tag{2}$$

where: $\langle\rangle$ denotes the averaging over all molecules, and β is an angle between a particular molecule director and the averaged orientation of all molecules. The S parameter for full ordering (each molecule is oriented in the same direction) is equal to 1, while the isotropic state is equal to 0. Typically, LCs exhibit the S parameter in the order of 0.3–0.8 [37].

Depending on the spatial ordering of molecules, one can distinguish the following phases:

(a) Nematic phase – The lowest ordering characterizes this type of mesophase among other LCs phases. They exhibit no pattern in the alignment of molecules; the ordering is only referring to molecule directors, which are evenly oriented in the whole phase. The nematic phase is schematically presented in Figure 4(a). Nematic LCs, due to the relatively low viscosity and existence in an extensive range of temperatures, are the most popular in industrial applications.

(b) Smectic phase – This type of mesophase is more ordered than the nematic phase. The center of molecular masses composing smectics is organized in planes. Depending on the type of smectic phase, the molecules might be oriented along with the layer normal (Smectic A – SmA) or tilted by a certain angle (Smectic C – SmC). Within the layer, some smectics can exhibit the ordering of molecules in hexagonal symmetry.

Some of them can have molecules aligned with layer normal (Smectic B – SmB) or be tilted (Smectic F – SmF and Smectic I – SmI). The schematic representation of SmA is shown in Figure 4(b).

(c) Cholesteric phase (ChLC) – This type of mesophase exhibits chirality in molecule alignment. In general, in the cholesteric phase, molecules assigned to consecutive layers are slightly rotated relative to the previous phase. After a certain distance called the pitch *P*, their orientation is once again the same. The whole pattern is periodical, and if the size of the pitch is of the order of light wavelength scale, the cholesteric phase can exhibit a photonic stop band. Sometimes cholesteric LCs are called chiral nematics. A schematic representation of the cholesteric phase is shown in Figure 4(c).

(d) Chiral smectic phases – This type of mesophase is quite similar to the cholesteric phase. However, it is much more ordered relative to previous phases. The chirality results from the alignment of molecules, which direction is rotating along the cone's lateral surface (see Figure 4(d)) as an example of chiral smectic phase C – SmC* (asterisk indicates that particular smectic phase is chiral). Chiral smectic phases frequently exhibit ferroelectric or antiferroelectric properties, and for that reason, they are now widely investigated for use in fast electro-optical switches [40].

(e) Blue phases – These phases exhibiting chirality in three dimensions. Nowadays, we can distinguish three types of blue phases, blue phase I (BPI), blue phase II (BPII), and blue phase III (BPIII). The most essential "building block" of the two first types of blue phases, namely BPI and BPII, are so-called double-twist cylinders. The alignment of molecules inside such a cylinder is shown in Figure 4(e). In general, the molecules in the core of a cylinder are oriented along with them. However, the molecules' orientation is gradually rotating (twisting) when the core's distance is increasing. When molecules are rotated by +45 or –45° concerning molecules in the core, the cylinder reaches its' boundaries. At the distance of cylinder diameter, molecules form a twisted molecular alignment of length equal to a quarter of a pitch. Each cylinder has two perpendicularly oriented helices for each cross-section, forming a kind of cross-like structure. For BPI, the structure composed of a double-twist cylinder is cubic body-centered, for BPII is simple cubic, and BPIII is thought to be more likely amorphous [41]. The structural analysis of BPs shows that even in the case of more ordered BPI and BPII LCs; it is impossible to pack the double twist-helix without the formation of disclinations. Thus, both blue phases consist of defects, which are presented in Figure 4(e). The BPs are natural, chiral photonic crystals; thus, they are subject to intense scientific studies. However, their thermodynamic stability is relatively low. They occur in a very narrow range of temperatures, and the issue related to the stabilization of BPs remains a challenge.

To summarize, LCs exhibit many beneficial properties that could be controlled by external factors. They are useful in optical applications. Moreover, LCs are resistant to optical damage; thus, they can be utilized together with laser beams. Due to the liquid-like behavior, LCs can be easily functionalized by the addition of dye molecules. Thus, they can gain additional desired properties.

4 Band edge lasers

Photonic band-gap (PBG) systems are periodic dielectric structures composed of alternating high and low permittivity materials [42]. Band gaps in materials are essential for waves propagating in regular periodic structures and arise essentially from interference effects between such waves. A variety of potential applications of PBG have been shown, such as lasers, transistors, single-mode LEDs, and solar cells. This chapter is concerned with PBG LCs in which the periodic dielectric structure can be used to generate laser light.

4.1 Cholesteric

The main features that make cholesteric liquid crystal lasers (ChLCL) very attractive for photonic applications are the ease of fabrication and tuning the emission wavelength by using different angle pitch gradients, by changing the composition [43, 44], via external stimuli such as electric field [45], temperature [46], or mechanical strain [47].

In 2010, Uchimura et al. [48] reported how the proper design of laser dyes is important to realize low-threshold dye-doped ChLCL to achieve continuous-wave (cw) operation, the ultimate goal of LC lasers. The lasing spectra of pyrene-derivative-doped ChLCL were observed at the high energy edge of the photonic band-gap, which is an unusual phenomenon and is attributed to the orientation of the transition dipole moment of the dye molecules. These results should serve as guidelines for designing new dyes to lower the threshold of LC lasers. Aggregation-induced-emission (AIE) dyes have also been used as a gain material.

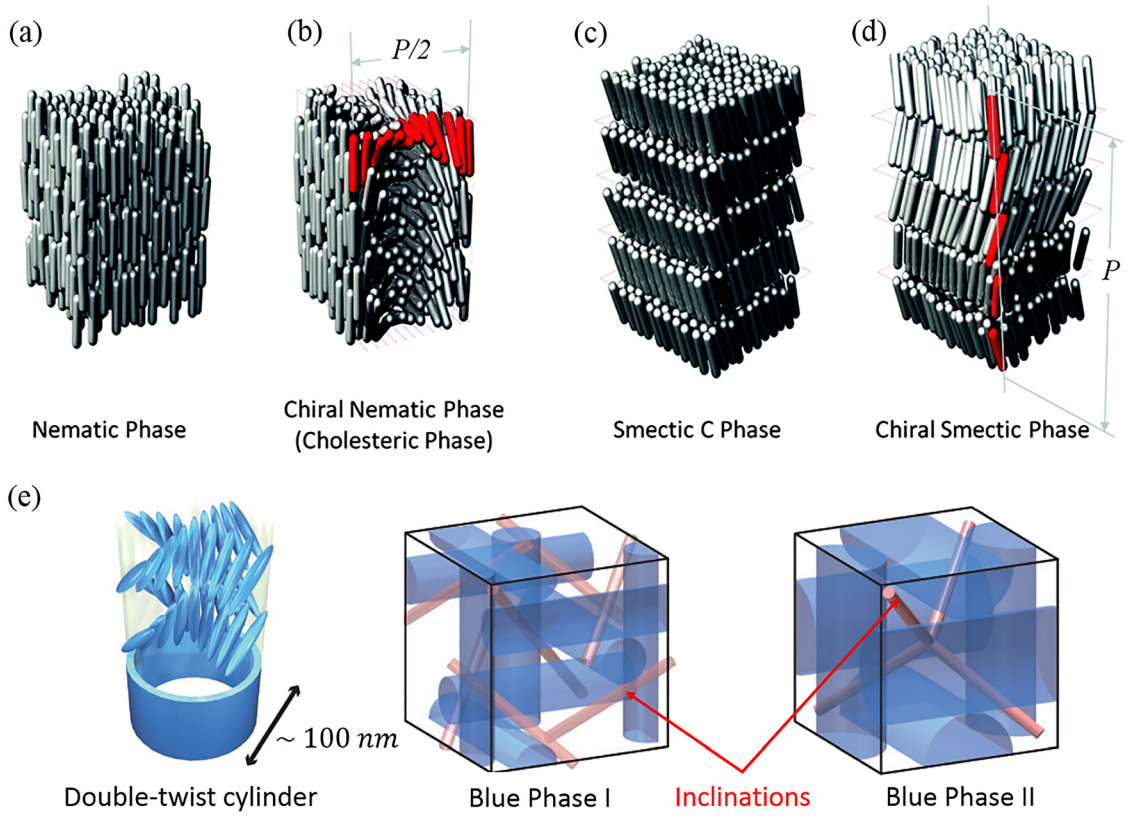

Figure 4: Schematic representation of molecules ordering in different types of LC phases: nematic phase (a), cholesteric phase (b), smectic C phase (c), chiral smectic phase (d), and two types of blue phases, namely BPI and BPII with molecules arrangement in double twist cylinder – a basic building block for blue phases (e). Drawings (a)–(d) adapted from [38], (e) adapted from [39].

Wang et al. [49] have shown that such AIE dye-doped ChLC is capable of lasing action with huge Stokes shift (250 nm) at a moderate threshold (600 μJ/mm^2), which could be further reduced with optimization in AIE dye concentration, sample thickness, input optics, and selection of other AIE materials. Furthermore, the sample is highly photostable without noticeable degradation of performance. To conclude, AIE dyes are promising to gain media for a variety of laser hosts.

The novel BODIPY based red emitter (4,4-difluoro-2,6-di(4-hexylthiopen-2-yl)-1,3,5,7,8-pentamethyl-4-bora-3a,4a-diaza-sindacene) was also employed as a ChLC laser dye [50]. A new construction method in which a flat capillary filled with an optically isotropic dye solution is sandwiched between two dye-free planar ChLC cells was described. Such construction provides optically pumped lasing at the same wavelength as in the classical scheme of a dye-doped planar ChLC cell. Facile assembly/disassembly of the capillary laser can be useful for optimizing laser characteristics using small amounts of dye and ChLC, which can be used as a simple method to explore new active laser media and optimize the concentration dependencies of the lasing parameters.

In 2014, authors first described an optically stable and tunable laser using a quantum-dot (QD) embedded cholesteric liquid crystal (QD-ChLC) microresonator with an added chiral-azobenzene moiety [51], which possesses optical stability and tunability. The tunable spectral ranges in the PBG and lasing wavelength of the QD-ChLC composite cell are over 60 and 40 nm, respectively. Because of the high stability and optical and electrical dual-excitability of the QDs, the QD-ChLC has a high potential to develop multiway drivable coherent QD light sources or lasers with highly flexible tunability, high stability, and reliability.

An azo-chiral dopant was also used by Lin et al. [52]. This study first demonstrates a spherical microlaser with optical tunability and switchability based on a dye-doped cholesteric liquid crystal (DDChLC) microdroplet with an azo-dye. The spherical microlaser's lasing wavelength can be tuned from 563 nm up to 586 nm by increasing the irradiation time of a weak UV beam. This tunability is attributed to the slow *trans-cis* isomerization of the azo-chiral dopant induced by weak UV irradiation. The microlaser can be switched on by the blue beam irradiation-induced *cis-trans* back-isomerization of the azo-chiral dopant following the

intense UV irradiation. The three-dimensional DDChLC spherical microlaser is a highly promising controllable 3D microlight source or microlaser for applications of 3D all-optical integrated photonics, laser displays, biomedical imaging, and therapy, and as a 3D UV microdosagemeter or microsensor.

In 2010, Humar and Musevic [53] published pioneering work about 3D lasing from dye-doped cholesteric microdroplets with a Bragg-onion configuration of the refractive index. The lasing wavelength was determined solely by the cholesteric pitch. The laser light was emitted from the center of the ChLC microdroplet in all directions. Thus, the laser is acting as a coherent, point-like, and omnidirectional light source, where the emission wavelength is tunable by changing the temperature. The tuning range is several tens of nanometers. Since then, many other interesting papers have been published about the 3D ChLC omnidirectional photonic structures and their applications in lasing, including core–shell structures [54–60].

A wide-range electrically tunable laser based on dye-doped polymer-stabilized cholesteric LCs (PSChLCs) with negative dielectric anisotropy was described by Lu et al. [60]. The laser's wavelength could be tuned reversibly in a wide spectral range, from 558 to 673 nm, by controlling the pitch gradient through DC electric fields (Figure 5).

The electrically controlled PSChLC laser's principal advantage is that the electric field is applied parallel to the helical axis and changes the pitch gradient instead of rotating this helix axis, thus preserving the heliconical structure during lasing [45]. The PSChLC laser, with advantages including a wide tunable range, self-restoration, and rapid response and stability, coupled with its miniature size and narrow linewidths, has diverse applications in intelligent optoelectronic devices.

In 2017, Lin et al. [61] reported that PBG reflectivity could be tuned over nearly the full visible region based on a gradient-pitched enantiomorphic ChLC polymer template refilled with a nematic LC (NLC) or dye-doped nematic LC (DDNLC) (Figure 6). The sample is formed by suitably merging two oppositely-handed gradient-pitched templates and then refilling the DDNLC with a fluorescence distribution covering almost the entire visible region. The experimental results show that the high reflective PBG tuning range is spanning from 450 to 750 nm. The lasing output with simultaneous right- and left-circular polarizations can be tuned from the blue to the red region (483.2–633.7 nm).

The same research group has shown that the PBG can be spatially tuned over the entire visible region, and the lasing is thermally convertible between single-mode and multimode nature [62].

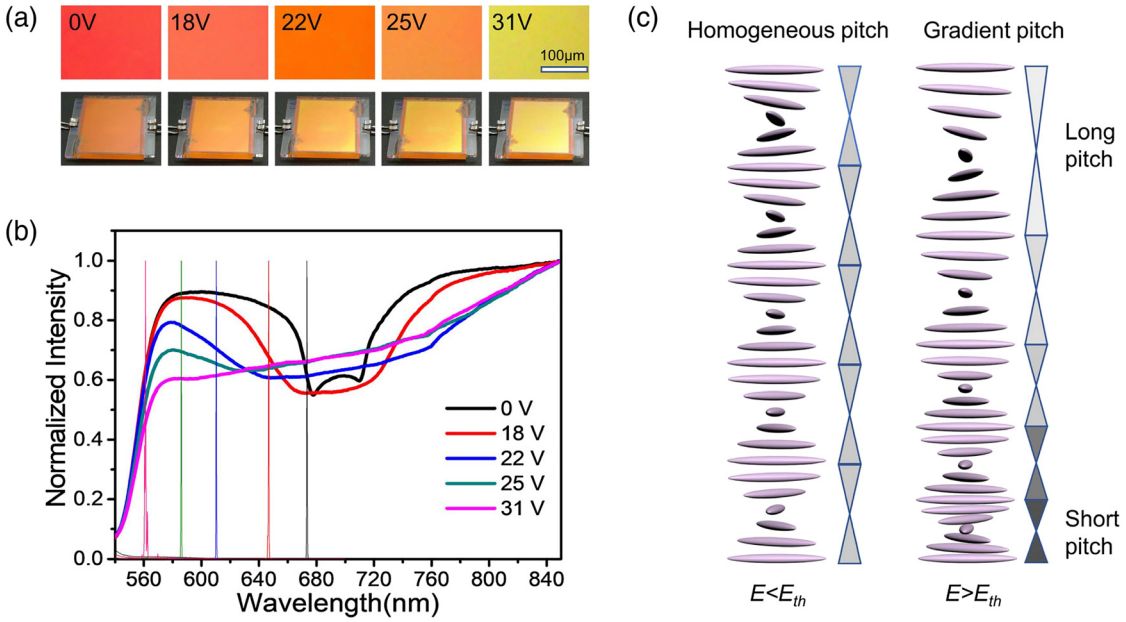

Figure 5: The electric-field-dependent broadening of the selective reflection band and the electrical tunability of the laser's emission wavelength.
(a) The microphotographs observed under a polarized optical microscope and photographs of the dye-doped PSChLC under various voltages, (b) the transmission and corresponding laser emission spectra of the dye-doped PSChLC under various voltages with excited pump energy of ~1.4 μJ, and (c) the schematic illustration of the pitch distribution under different electric fields [60].

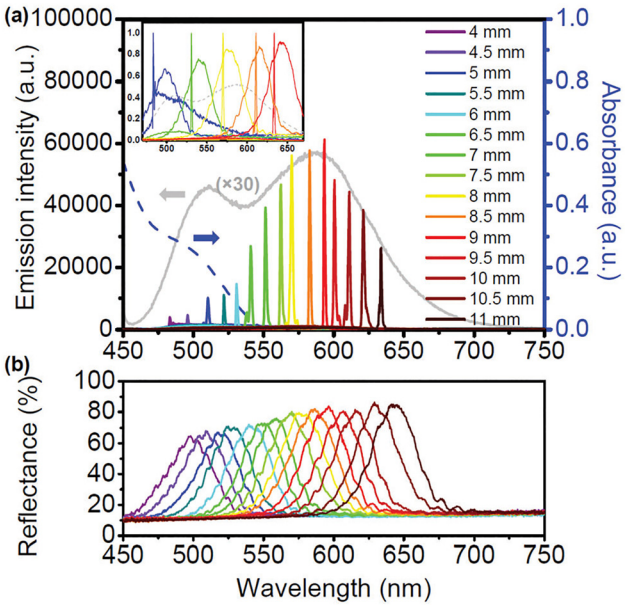

Figure 6: (a) Lasing emission spectra of the DDNLC-refilled gradient-pitched enantiomorphic template sample at $E = 4.56$ mJ per pulse, measured at positions from $x = 4$ mm to $x = 11$ mm, at $T = 48$ °C. The inset in (a) shows the reflection bands with the associated normalized lasing lines measured at five selected positions in the DDNLC-refilled gradient-pitched enantiomorphic template sample. The grey and blue dotted curves in (a) are the measured fluorescence emission and absorption spectra of the DDNLC, respectively, in the isotropic state for reference. (b) Corresponding reflection spectra of the sample measured at positions from $x = 4$ mm to $x = 11$ mm at 48 °C [61].

Finally, lasing from cholesteric liquid crystal elastomer (CLCE) films, both in glassy and rubbery states, with a dramatic reversible blue-shift of the selective reflection band from near IR to near UV ranges of the spectrum, was achieved by a novel mechanical compression of the CLCE film using uniaxial strain along the helical axis. Using an accurate measurement scheme based on volume conservation of the CLCE film, it was shown, for the first time, that both the helical pitch and the wavelength of laser emission from the CLCE film in the rubbery state are linearly dependent on the mechanical strain applied to the film [47].

4.2 Blue phase

The liquid-crystalline BPs appearing between the Ch and isotropic (Iso) phases have attracted particular attention owing to their unusual self-assembled cubic structures and unique optical characteristics. These structures comprise double-twist cylinders (DTCs) and vary depending on how the DTCs are assembled in three-dimensional space. These phases are known as cubic BP (BPI, BPII) and amorphous BP (BPIII), numbered in order of increasing temperature (Chapter 3). The cubic BP has a three-dimensional cubic symmetry with lattice parameters ranging from 200 to 300 nm, while the amorphous BP has an isotropic symmetry [63, 64]. BPs are optically active and isotropic, exhibiting a Bragg reflection due to their periodic structures. These characteristics, combined with the capability to shift the PBG in response to external perturbations, make BPs fascinating materials for applications such as tunable lasers, where laser emission can be realized in three orthogonal directions and can be obtained simultaneously using the three-dimensional PBG.

A spatially tunable PBG of wide spectral range and lasing emission based on BP and dye-doped blue phases (DDBP) wedge cells, respectively, was demonstrated for the first time in 2014 [65]. The wedge cell's gradient thickness provides different boundary forces to the LC molecules, hence achieving the continuously spatial shifting reflections of BP in the wedge cell. The continuously shifting reflection was more than 130 nm, nearly covering the range of blue, green, and red regions. Based on the tunable PBG of the wedge cell, a spatially tunable laser based on a DDBP wedge cell was also demonstrated, where the lasing wavelength is continuously tunable within a spectral range of about 68 nm (Figure 7). Both the tuning ranges of PBG and lasing emission are broader than those of CLC and DDCLC wedge cells.

Numerous efforts have been put to develop new BP materials that exist over an inherently wide range of temperatures [64, 66]. In 2015, highly tunable 3D liquid photonic crystals were demonstrated using low-dc-field-driven polymer-stabilized blue phase LCs [46]. The photonic band-gap's central wavelength can be reversibly shifted to more than 200 nm away from the original position (Figure 8). Besides, by controlling the polymerization-induced morphology variations, the band-gap can also be expanded from a bandwidth of around 30 nm to at least 310 nm. Finally, in such a system, a "white" blue phase was observed for the first time, where shifting and expansion of PBG can be independently manipulated in any crystal axis without affecting the lattice spacings in the other dimensions (Figure 8).

Highly appealing work was published by Wang et al., where they report on an electrically tuning of the PBG that exhibits the dependence on the polarity of bias voltage in the polymer-stabilized blue phase I system through fabricating polymer network, with nonhomogeneous density distribution from top to bottom across the cell gap. A tunable PBG [67] across the entire visible spectrum was achieved with a hypsochromic shift under negative bias and a bathochromic shift under positive bias.

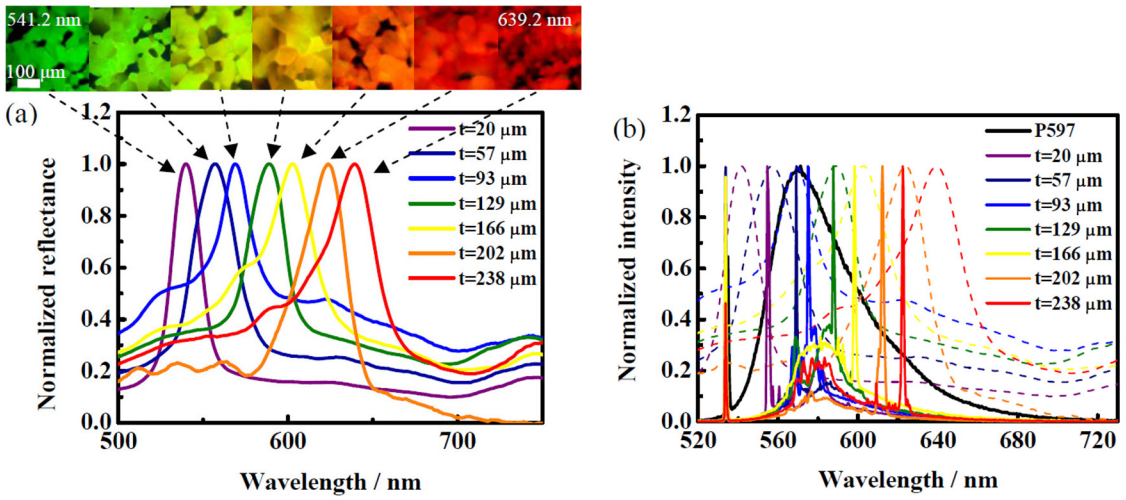

Figure 7: (a) Measured reflection spectra and corresponding R-POM BP images for the DDBP wedge cell at $y = 2.5–28.5$ mm ($t = 20–238$ μm) at 54.5 °C. (b) Measured lasing spectra (solid curves with sharp peaks) and corresponding reflection spectra (dotted curves, same as those shown in (a)) for the DDBP wedge cell measured at $y = 2.5–28.5$ mm ($t = 20–238$ μm) at 54.5 °C. The black solid curve is the fluorescence emission spectrum of the laser dye [65].

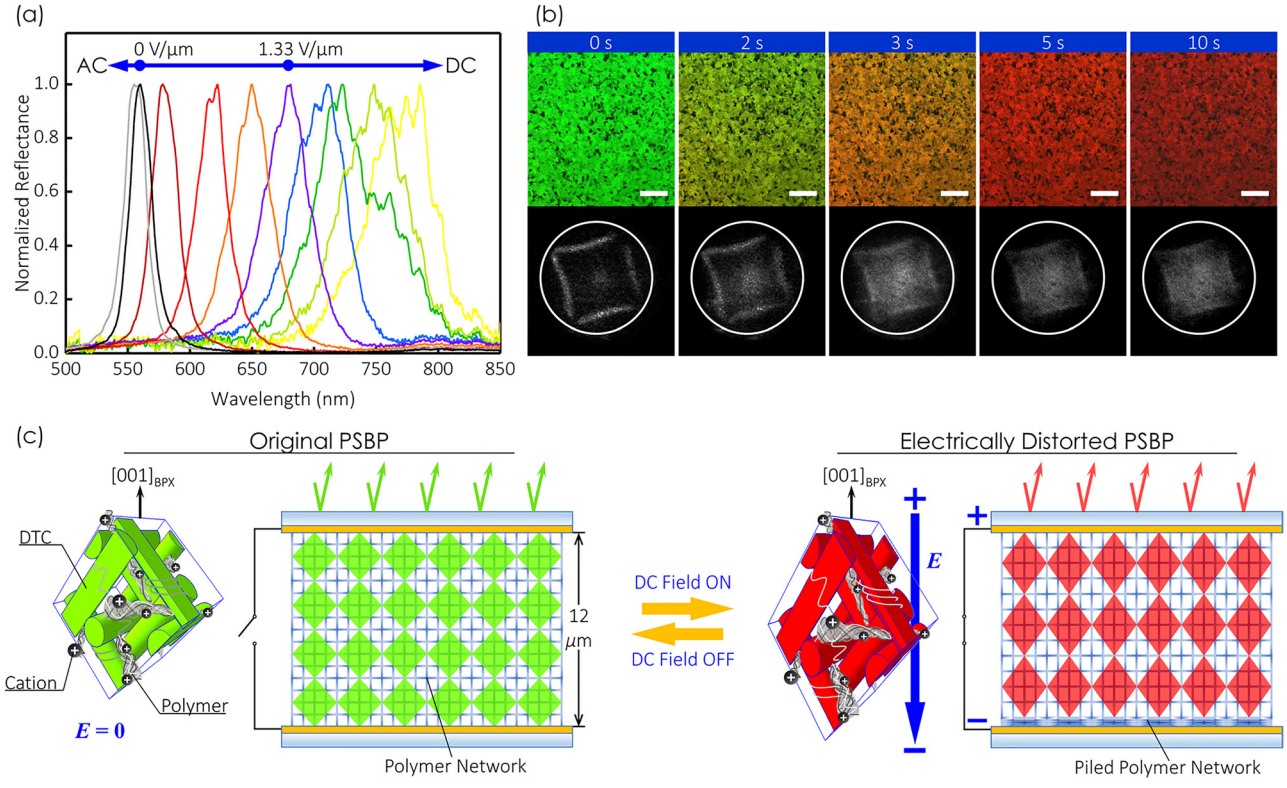

Figure 8: Red-shift of the photonic band-gap.
(a) normalized reflection spectra of a 12-μm thick PSBP film in various DC fields (0–2.67 V/μm) and an AC field (5.83 V/μm). (b) Time-resolved microscopic images (top, scale bars: 100 μm) and Kössel diagrams (bottom) captured under a DC field of 1.33 V/μm. (c) Schematics of the underlying mechanism for the DC-induced band-gap shifting in PSBP. The spectra were normalized to their peak intensities [46].

Another example of a polymer-stabilized blue phase (PSBP) photonic band-gap (PBG) device with a wide-band spatial tunability in the nearly entire visible region within a wide blue phase (BP) temperature range, including room temperature, was published by Lin et al. [68]. Such a device was fabricated based on the reverse diffusion of two

injected BP-monomer mixtures with low and high chiral concentrations and, afterward, through UV-curing. This gradient-pitched PSBP can show a rainbow-like reflection appearance in which the peak wavelength of the PBG can be spatially tuned from the blue to the red regions (165 nm) at room temperature.

Yan et al. have shown that freestanding, large-domain blue phase (BP) films based on self-assembly technology can be obtained [69]. This fabrication method enables the formation of BP domains with large-scale lateral dimensions of 230 nm, which exhibit sharp photonic bandgaps with high reflectivity. Additionally, they have shown that dual-wavelength lasing can be achieved by doping the large-domain BP films with fluorescent dyes, which was first observed in BP materials.

In 2018, Petriashvili et al. [70] demonstrated the laser emissions from BPII and BPI microspheres and the temperature-controlled laser tuning from the BPI microspheres. They have prepared BPs microspheres formed and emulsified in a Polyvinyl alcohol/water (PVA/water) environment. Due to the temperature-dependent selective reflection of BPI, the temperature-controlled lasing tuning of about 55 nm was obtained.

Finally, in 2018, Gandi et al. presented the first photonic device based on amorphous BPIII by demonstrating that a three-dimensional BPIII polymer scaffold or template, when infiltrated with liquid crystal and laser dye, forms a system where random lasing action is generated due to multiple scattering events occurring in the nanoporous and disordered polymer replica of BPIII [71]. This study represents a facile approach for developing photonic devices, favorably exploiting unique polymer network morphologies for laser emission. Information about blue phase liquid crystalline lasers is gathered and presented in Table 1.

4.3 DFB

The distributed feedback (DFB) based lasers were constructed for the first time 10 years after the ruby laser development. What is typical for the DFB lasers, and what distinguishes them from the other type of lasers, is a specific resonator shape. Instead of the classical system with two external mirrors, the feedback is provided by a periodic structure with modulation of refractive index and/or gain coefficient. In the last decade, tunable DFB lasers have attracted significant attention because of their great promise in applying modern technologies such as tunable optical sources, biosensors, and optical communication. According to the Bragg condition, the emission wavelength can be tuned by adjusting the periodicity or effective refractive index of the grating. Several DFB lasers that are tunable by changing the grating period have been demonstrated using methods of electrically or mechanically stretching the grating periodicity [74, 75], two-beam holography [76], and in a spatial gradient of film thickness or grating period [77]. Because of the high efficiency of the refractive index modulation of LCs, incorporating LC material into the DFB resonant cavity is one of the most

Table 1: Blue phase liquid crystalline lasers.

LC matrix	Dye	Tuning range	Temperature	Electric field	Lasing Threshold	Ref.
PSBPI	DCM or PM597	~20 nm ~20 nm	RT	0–2.5 V/μm	1 μJ/pulse at l = 631.2 1.9 μJ/pulse at l = 601.5	[67]
BP1	Pyrromethene 597 Coumarin 153	55 nm 60 nm	64–80 °C 80–88 °C	N/A	2.6 μJ/pulse	[65]
BP (wedge sample)	P597	68 nm	54.5 °C	N/A	18–28 μJ/pulse	[65]
BP	PM 567 + azo chiral dopant	567–593 nm	RT	N/A	20–36 μJ/pulse	[72]
PSBP (gradient pitch)	(P597)	552.9–610 nm	RT	N/A	3.5–7 μJ/pulse	[68]
BPIII	DCM	600–640 nm (random lasing)	RT	N/A	~80 μJ/pulse	[71]
BPI	Oxazine-17 dye	~610–630 nm	35.3–34.7	0–2.3 V/μm	5 mJ/cm^2	[63]
BPI	P597	54–56 nm	50.2	0–44 V	90 μJ/pulse.	[73]
BPI (free standing)	Coumarin 6	530.6 and 516.2 nm (dual wavelength)	RT	N/A	2.68 nJ/pulse and 5.97 nJ/pulse	[69]
BPI and BPII (microspheres)	Coumarin 503, DCM	517–629 nm	22.15–24.25	NA	2.8 mJ/cm^2 2.2 mJ/cm^2	[70]

promising ways to effectively tune the emission wavelength of the DFB laser [78].

As an efficient method to realize tunable lasers, holographic polymer dispersed liquid crystal (HPDLC) configurations have been developed. The HPDLC grating is fabricated by a mixture of LC and monomers exposed to two or multiple interfering laser beams. The monomers undergo a fast free-radical photopolymerization in the bright regions of the interference pattern; counter-diffusions of the LC and monomers are initialized due to the resulting concentration gradient and alternating layers of the polymer in the bright fringes, and the LCs are formed in the dark fringes [79]. The formed periodic structure can be regarded as a one-dimensional photonic crystal that an optical resonator for emitted lasers. In 2014, Diao et al. proposed an anisotropic waveguide theory for electrically tunable distributed feedback laser from dye-doped holographic polymer dispersed liquid crystal grating, where the period grating structure, optical anisotropy of the liquid crystal, and practical light propagation path in the HPDLC have been considered [80].

The same research group has demonstrated the electrical control of the DFB organic semiconductor laser based on an HPDLC [81] and giving a full optimization and characterization of the lasing performance of MEH-PPV activated HPDLC lasers [82].

As DFB resonator nanoimprinted ITO transparent electrode was also used, where together with LCs, successful tuning of lasing wavelength from an organic dye-doped LC laser by applying external voltage was observed (Figure 9) [83].

Since the reorientation of LCs by applying a voltage across the DFB resonator brought changes of the effective refractive indices of the guided mode, lasing emission from the LC laser with the nanoimprinted ITO electrode was tuned by 6 nm at a low voltage of 8.0 V. From these results; it is shown that the nanoimprinted ITO film simultaneously acts as a DFB resonator, a transparent electrode, and an alignment layer for LCs. The same research group described surface-emitting DFB lasers with the 2D nanostructured ITO films and dye-doped LCs. From the optical measurements for the LC lasers, it was proven that the energy transfer process between two organic dyes and highly ordered dye molecules in the LC host, together with strong optical feedback in 2D DFB resonators, reduces the lasing threshold. Additionally, it was shown that wide spectral tuning of laser emissions of ~26 nm in a single LC laser with a wedge-shaped ITO resonator could be obtained [84]. Such a tunable lasing device with a functional electrode gives rise to various opportunities and advances in tunable laser technology.

Nanoimprint UV lithography was also used to manufacture temperature sensors based on thermally tunable dye-doped LC (DDLC)/polymer-grating DFB laser based on an LC-covered polymer grating with nano grooves [85]. The surface-emitting DFB laser's lasing wavelength can be tuned from 625.1 to 606.35 nm by varying the temperature from 10 to 50 °C. This thermal tunability is attributable to the temperature sensitivity of the effective refractive index of the LCs in the laser. Several other studies on lasing for dye-doped 2D HPDLC quasicrystals have been reported. Li et al. reported multimode lasing from the microcavity of an octagonal quasicrystal [86]. Luo et al. have investigated the lasing from Penrose quasicrystal with excellent linear polarization and low threshold [87], as well as the temperature effects [88]. They have also shown the studies on lasing from organic nanostructure quasicrystals formed by seven- or nine-beam interference using low contrast material. The wavelengths of the lasing peak were determined by both the local structure of the quasicrystal that the

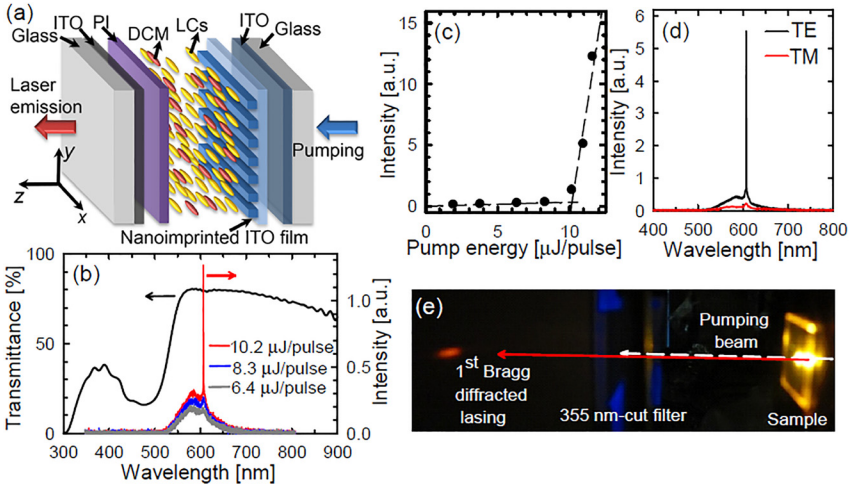

Figure 9: (a) Schematic illustration, (b) transmission and emission spectra at different pumping energies, (c) threshold behavior of lasing emission intensity, (d) polarized lasing emission spectra at the pumping energy of 11.6 μJ/pulse, and (e) photograph of far-field emission pattern of the surface-emitting DFB laser with the nanoimprinted ITO electrode and dye-doped LCs [83].

pumping light experienced and the photoluminescence of laser dye-doped [89].

In 2012, Diao et al. described an organic dual-wavelength DFB laser empowered by a dye-doped HPDLC grating [90]. The dual-wavelength laser operates at 586.6 and 670.2 nm simultaneously in one laser beam via the seventh and eighth Bragg orders of a one-dimensional (1D) HPDLC grating with a special period (Figure 10).

Stable tri-wavelength laser emission (625.5, 617.4, and 614.3 nm) at six different directions was observed by Huang et al. A continuously tunable multiwavelength polymer laser is based on a triangular lattice photonic crystal cavity, which was initially fabricated through multiple interference exposure and was then replicated into a low refractive index polymer via UV-nanoimprinting. The blend of a blue-emitting conjugated polymer and a red-emitting polymer was used as the gain medium. Working behaviors are explained by the grating diffraction theory as the triangular-lattice photonic crystal cavity could be regarded as a combination of three 1D DFB lasers.

Such a mirrorless laser with a simple fabrication process, low cost, and possible tunability due to the excellent optoelectronic response of LCs make holographic polymer dispersed liquid crystal (HPDLC) photonic quasicrystal promising for a new type of all miniature organic lasers.

4.4 VCSEL and other types

Vertical Cavity Surface Emitting Lasers (VCSELs) have been used as light sources in optoelectronic devices in the past decades, mostly in optical interconnects and sensing applications. It has been demonstrated that the properties of the emitted light can be controlled, in both wavelength [91, 92] and polarization [93], by using an LC layer in combination with a VCSEL. An applied voltage controls the LC's orientation in the layer and this, in turn, changes the optical path length of a beam propagating through the LC layer. The main advantage of the tunable LC-VCSELs is the use of liquid crystal technology, which is well established and, therefore, cost-effective. Moreover, LC being enclosed within the structure makes the device robust and reliable, in contrast to MEMS technology requiring moving mirrors suspended in the air.

In 2018, Frasunkiewicz et al., by performing one-dimensional transfer-matrix optical calculations supplemented with a fully-vectorial three-dimensional self-consistent modeling of thermal, electrical, and optical phenomena, have optimized the design of VCSELs and show the dependency of the emitted wavelength on LC cell thickness and the LC director orientation. The analysis is concluded with a possibility of achieving a 68.5-nm tuning range in a continuous-wave operation regime, without polarization or transverse mode switching [94].

Neyts et al. published a series of work showing that the laser emission and emission wavelength polarization can be controlled by applying an appropriate voltage over the liquid crystal layer [95–97]. A schematic illustration of VCSEL is shown in Figure 11 (left).

The experimental results show that the CLC-VCSEL has several advantages: (*i*) its circular polarization has a higher purity than the linear polarization of a stand-alone VCSEL; (*ii*) the threshold current is lowered; and (*iii*) the temperature-dependent emission wavelength can be tuned over a broader range within the same temperature interval. These properties can provide applications, which require higher polarization purity, lower energy consumption, and broader wavelength tuning [97]. In 2020, it was shown that CW operation at room temperature and 23.5 nm wavelength tunability could be obtained in 1.55 μm InP-VCSEL [99]. This device combines InP-based materials with LC microcells collectively fabricated and integrated on the surface of a half-cavity VCSEL.

Finally, Lin et al. demonstrated, for the first time, an electrically tunable LC-polymer composite laser with a symmetric sandwich structure. This novel device consists of two identical polymer-stabilized cholesteric liquid-crystal layers as a distributed Bragg reflector (DBR) cavity and a dye-doped nematic liquid crystal (DDNLC) layer as

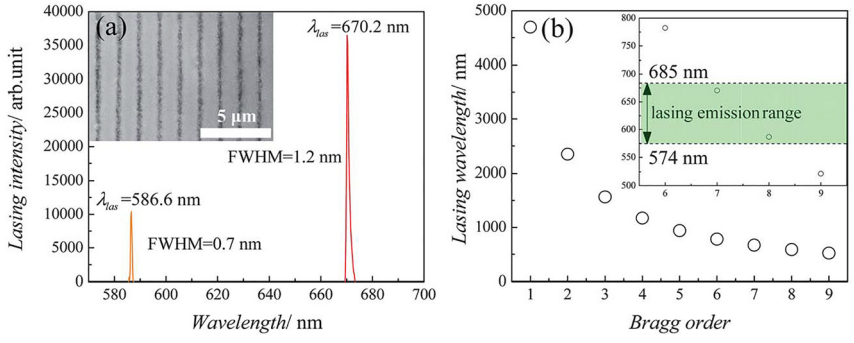

Figure 10: (a) The lasing spectrum of the dual-wavelength laser and (b) the calculated lasing wavelength positions of the DCM-doped HPDLC grating with a period of 1520 nm for different Bragg orders. The inset in (a) is the SEM image of the grating, and the inset in (b) is an amplification of the data from the 6 to 9 Bragg orders [90].

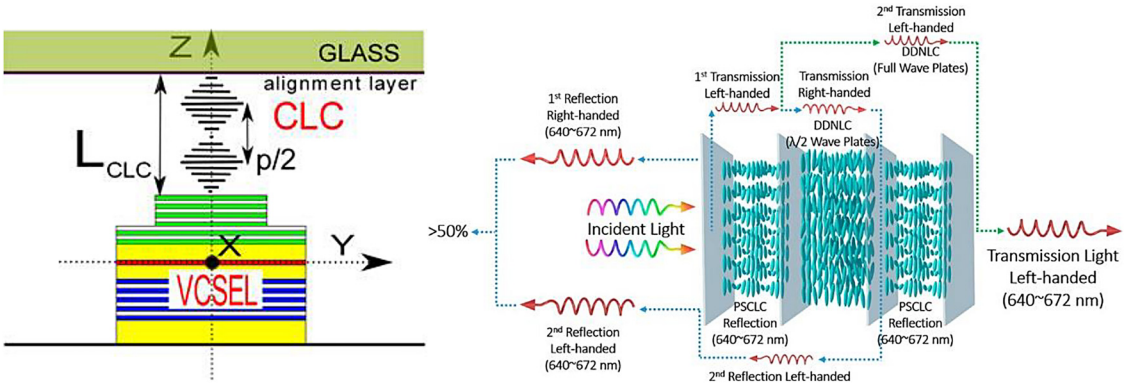

Figure 11: (left) Schematic of VCSEL with CLC overlay: the LC cell is closed from the top by a glass plate with a deposited LC alignment layer [83]. (right) Schematic of the LC-polymer composite laser with a symmetric sandwich structure in which a dye-doped nematic liquid crystal (DDNLC) layer is sandwiched between two polymer-stabilized cholesteric liquid-crystal (PSCLC) layers [98].

the gain medium and half-wave plate sandwiched between the PSCLC layers (Figure 11 (right)) [98].

By simultaneous application of an identical DC voltage on the two PSCLC layers, the helical pitch within PSCLCs is elongated and compressed at opposite sides to form a pitch gradient (because of the electrically induced ion concentration gradient), thereby leading to a widened PBG. Given the electrically induced broadening of the PSCLC reflection band, the amount of the resonant modes and lasing wavelength of the sandwich LC-polymer composite laser can be controlled by the DC voltage. This device provides new insights into tunable LC lasers and can be potentially applied in sensors, medical imaging, displays, and light sources, among others. Given the proper designs of the gain profile and resonant modes and simultaneous generation of red, green, and blue lasing emissions, even an electrically controllable white-light laser can be anticipated.

5 LC random lasers

5.1 Nematic

Thanks to the unique properties of the LCs in the nematic phase, they constitute great potential if we consider the laser action in disordered organic systems [100]. The main structural difference among typical anisotropic media, which provides constructive light diffusion, is the molecular arrangement. Rod-like architectures, oriented along with the director $n(r,t)$, make this uniaxial liquid as the particular medium, which can fluctuate and provide light diffusion on about 10^6-times higher than other, well-known isotropic liquids. Spontaneous director fluctuations represented by [100]:

$$n(r,t) = n_0 + \delta n(r,t) \tag{3}$$

leads to further fluctuation in the local dielectric tensor, consequently [100]:

$$\epsilon_{\alpha\beta} = \epsilon_\perp \delta_{\alpha\beta} + (\epsilon_\parallel - \epsilon_\perp) n_\alpha n_\beta \tag{4}$$

Such an effect is responsible for multiple light reflections and diffusion, which provides optical feedback for stimulated emission.

Temperature is another parameter that can noticeably affect the random lasing action in NLCs [101]. This issue is strictly connected with a dedicated application. Because the nematic phase (as the other ones) is involved with the well-working temperature regime, it is important to maintain the proper environment. The nematic phase can be easily modulated by adjusting the heat flow [102]. A luminescent dye has to be implemented in such a system as well to achieve laser action. Then, one of the most critical parameters is LC and dye compatibility (chemical structures resemblance) [103]. In such a case, since the considered dye can be well-mixed with the branched matrix, it prevents additional light diffraction, which is an essential parameter in the random lasing phenomenon. Such compatibility is advantageous because only one component provides and, at the same time, limits all kinds of light diffusion contribution, which is easily controllable [104]. Furthermore, also electric [105] or magnetic [106] fields can change NLC architecture, and the effect provides various light diffusion [4]. However, the LC cell construction type (planar or homeotropic) influences the optical response coming from the material. If we consider nematic LC, the planar texture is preferred. Strangi et al. have recently presented the first observation of random lasing action from NLC (BL001) doped with pyrromethene 597 luminescent dye [107] (Figure 12(a)).

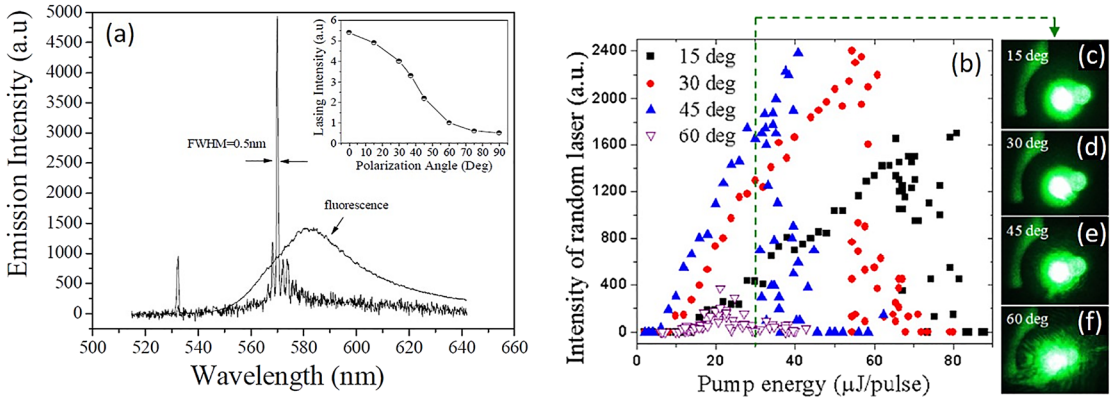

Figure 12: Fluorescence and lasing spectra are reported. Discrete sharp peaks emerge from the residual spontaneous emission for pump energy of about 1.2 μJ/pulse.
The inset shows the lasing intensity's dependence on the angle θ between the linearly polarized light and the local nematic director orientation [94] (a). The output intensity of random lasing versus the input pump energy at different incident angles θ with a fixed lateral section of the pump pulse on the NLC film $S' = 0.040$ mm^2 (b); Transmitted laser spots of the pump pulse with pump energy of about 30 μJ/pulse obtained at θ of (c) 15°, (d) 30°, (e) 45°, and (f) 60° [108].

Above the lasing energy threshold, which in that case was very low (~900 nJ/pulse), the discrete sharp peaks (FWHM = 0.5 nm) typical for RL were obtained. As the experimental proof that the observed emission has STE character, the authors performed a lasing intensity vs polarization angle investigation (inset of Figure 12(a)). It is seen that NLC doped with luminescent dye can provide efficient and polarization-sensitive RL, where the orthogonal direction causes an almost diminishing of the lasing action. In the same contribution, the authors have compared the NLC random laser energy threshold with two other, well-known lasing systems. The cholesteric liquid crystal (ChLC) [8, 109, 110], as an example of a well-ordered dye medium (thanks to the periodic helical structure of the matrix), characterizing the lowest energy threshold to obtain random lasing (~1 μJ/pulse). Disordered media was represented by a methanol solution with dispersed ZnO nanoparticles [111], which achieved the RL energy threshold a few times higher (~8 μJ/pulse). A partially ordered system contributed by nematic LC placed the energy threshold values close to the ChLC one, at ~2 μJ/pulse. The authors concluded that random, partially, and fully ordered systems provide various light scattering mechanisms leading to the random lasing modes.

Fengfeng et al. have investigated the pump beam intensity and angle influence on the RL nature, efficiency, and energy threshold values in highly concentrated DDNLC systems [108]. Due to the NLC domain's mobility controlled by an electric field direction from electromagnetic wave, a strong correlation between incident beam angle and LC cell positioning was proven, which resulted in different RL intensity and energy threshold values (Figure 12(b)). The authors also noticed that changing the incident laser line angle from the normal of the LC cell surface by 15, 30, 45, and 60° results in various energy threshold values, namely 3.7, 2.1, 1.4, and 2.5 μJ/cm^2 respectively. This means that the emission properties depend on the NLC director reorientation caused by the delivered electric field to the highly sensitive and easily controllable liquid crystalline domains. In other words, the photo-induced molecular fluctuations change the scattering conditions of the optically active NLC-based systems, which directly influence the random lasing feedback and loss parameter.

It was also proven that independently of the dye concentration, after a gradual increase of the pump beam intensity, there is a particular I_{pump} value, where output RL signal drops. However, the random lasing intensity corresponds to the various incidence angle, which is the highest for θ = 30 and 45° (abrupt slope, the lowest energy threshold values), then lower for θ = 30 and 60°, respectively. The last-mentioned laser configuration gives about a six-times lower random lasing feedback than marked in blue in Figure 12(e): θ = 45° configuration.

Huanting et al. have proven that using a very low DC voltage makes it feasible to modulate random lasing intensity due to the long-range NLC fluctuation and dielectric tensor changes [112]. Chia-Rong et al. have shown the possibility of RL intensity modulation in DDNLC even below the *Fréedericksz* transition threshold, which paved the way for ultra-low energy consumption for random laser emission control [113]. The polarization influence of the generated RL in DDNLC has also been reported in the literature [114]. Ji-Liang et al. have shown that sphere-phase nematic liquid

crystal in the shape of 3D twist architectures are more efficient (due to the fewer values of the RL energy threshold and lack of any pretreatment processing) than the typical chiral NLC structures [115, 116]. However, the dye-doped (PM597) chiral NLC generating discrete and narrow (FWHM = 0.3 nm) random laser modes, without rubbing procedure of the utilized soft mater, was recently reported [117]. The authors have proven that LC cell thickness has a significant impact on the RL energy threshold value. To conclude, the NLC-based random lasers constitute an easier and cheaper alternative for the classical lasers, where microcavities have to be prepared with ultra-high precision [118, 119].

5.2 PDLC

Polymer-dispersed LCs (PDLCs) are a class of organic materials that shows interesting electro-optical features (reversible switching processes) and highly optical anisotropic light diffusion [120]. In other words, PDLC materials characterize at the same moment both solid-state properties typical for polymers and specific fluid-like behavior related to the soft matter (LCs). A typical photo-initiated polymerization is used to create such bi-component architecture. A homogenous mixture of monomers and LCs react together under controlled conditions and create polymer-dispersed LCs. The polymerization environment has a significant impact on the final PDLC features [121]. PDLCs have many practical applications. However, they are mainly known as components for active walls [122]. There are two types of electrically controlled wall transparency. The first is called direct-mode PDLC. When the electric field is applied, the refractive index from polymer and LC is equal, and a match condition is achieved. In that situation, such material is fully transparent for visible light [123]. The second kind works exactly the opposite. The reverse-mode polymer-dispersed LCs have a milky structure when the applied electric field is provided. So, in the stationary state, the reverse-mode PDLCs are transparent and do not need any stimuli to sustain such conditions [124]. However, the first working random laser based on the dye-doped polymer-dispersed LC material (DDPDLC) was reported by a group of Wiersma in 2004 [125]. After that, the optical gain observed in disordered media based on the PDLC materials has attracted attention from many research groups [126].

Lihua Ye et al. have presented randomly arranged (nonoriented) and one-side aligned (oriented) dye-doped polymer-dispersed liquid crystal (N-DDPDLC, P-DDPDLC, respectively) systems [127]. These authors investigated macromolecular reorientation influence on the optical feedback parameters in the manner of random lasing emission. The authors found that the N-DDPDLC system characterizes the RL energy threshold on about 4.1 μJ/pulse; however, the achieved light amplification had a multimode (noncoherent) nature (FWHM ~0.5 nm). Whereas, for the P-DDPDLC system, several sharp laser spikes were observed (FWHM ~0.2 nm) and E_{th} = 3.5 μJ/pulse. The signal-to-noise ratio in the second case was huge, and distinct laser modes were well-separated. The results discussed above relate to an LC cell with an estimated thickness of 20 μm. When the samples were prepared according to the same protocol, although the thickness parameter has changed (d = 10 μm), the difference between nonoriented and oriented PDLC systems was even higher. The N-DDPDLC characterized similar behavior as previous LC cell constructions (multimode RL with FWHM ~0.5 nm and E_{th} = 3.0 μJ/pulse). Interestingly, the P-DDPDLC system gave even better results. Namely, the RL energy threshold was estimated at ~1.9 μJ/pulse. The optical cavity length was determined for the set of thinner samples due to the methodology (PFT analysis) introduced by Polson et al. [128]. The results gave the following numbers: L = 16.07 and 26.21 μm for nonoriented and oriented structures, respectively, which means that the optical path length in both cases was longer than the active layer thickness. The P-DDPDLC sample, at about 2.5-times higher, indicates that molecular alignment in the PDLC systems has a significant impact on the RL optical feedback mechanism [127].

According to the typical experimental approach, when LCs-based systems had been successfully enhanced (an increase of light diffusion and amplification) by nanoparticles (NPs), the same issue was concerned with the PDLCs materials. Zhen Zhen and co-workers showed a random laser based on the PM597 laser dye combined with manganese (II) chloride nanoparticles embedded in the same PDLC system [129]. As the reference material, the authors used pyrromethene 597 embedded in PDLC (without $MnCl_2$ nanoparticles). The effect of such an approach was as follows: RL energy threshold was estimated at about 7.57 μJ/pulse (FWHM = 0.23 nm) and 13.02 μJ/pulse (FWHM = 0.15 nm) for PDLC system with and without NPs, respectively. Also, the optical cavity length for the doped system is about 50% of the case without any $MnCl_2$ nanoparticles. The authors provided evidence that the addition of NPs to the PDLC system provided an extended lifetime of photons, which are present in the volume of the considered active and disordered architecture. Moreover, the energy transfer between nanoparticles and laser dye, which enhanced RL intensity, decrease its energy threshold, and allowed emission tunability.

A similar contribution is given by Long-Wu and Luo Gen, where a silver nanoparticle-doped PDLC system was recently reported [130]. PDLC-DCM doped with Ag NPs characterizes 20-times stronger light amplification in the manner of random lasing emission (and FWHM of the distinct laser modes less than 0.2 nm) than in the case where only DCM dye was introduced. This confirmed the already known mechanism that liquid crystal domains deliver light diffusion and metallic nanoparticles provide electric field enhancement.

Long-Wu et al. have shown an influence on the zinc oxide nanoparticles on the RL abilities of the PDLC systems [131]. The authors have considered three types of the investigated systems: DDPDLC solution with (*i*) small-sized LC droplets, (*ii*) ZnO NPs, and (*iii*) only dye solution with ZnO capillaries (without macromolecular matrix and LC). The spectral characterization of the mentioned systems is presented in Figure 13(a).

It is visible that the emission band is red-shifted for the systems where ZnO NPs were added due to the PDLC-DCM system. Moreover, the nature of light amplification becomes more coherent, and a higher number of selected and favored laser modes is observed. The spectral narrowing is substantial above the RL energy threshold, which is also visible as an increase of the signal-to-noise ratio. The general conclusion from the above-discussed comparison

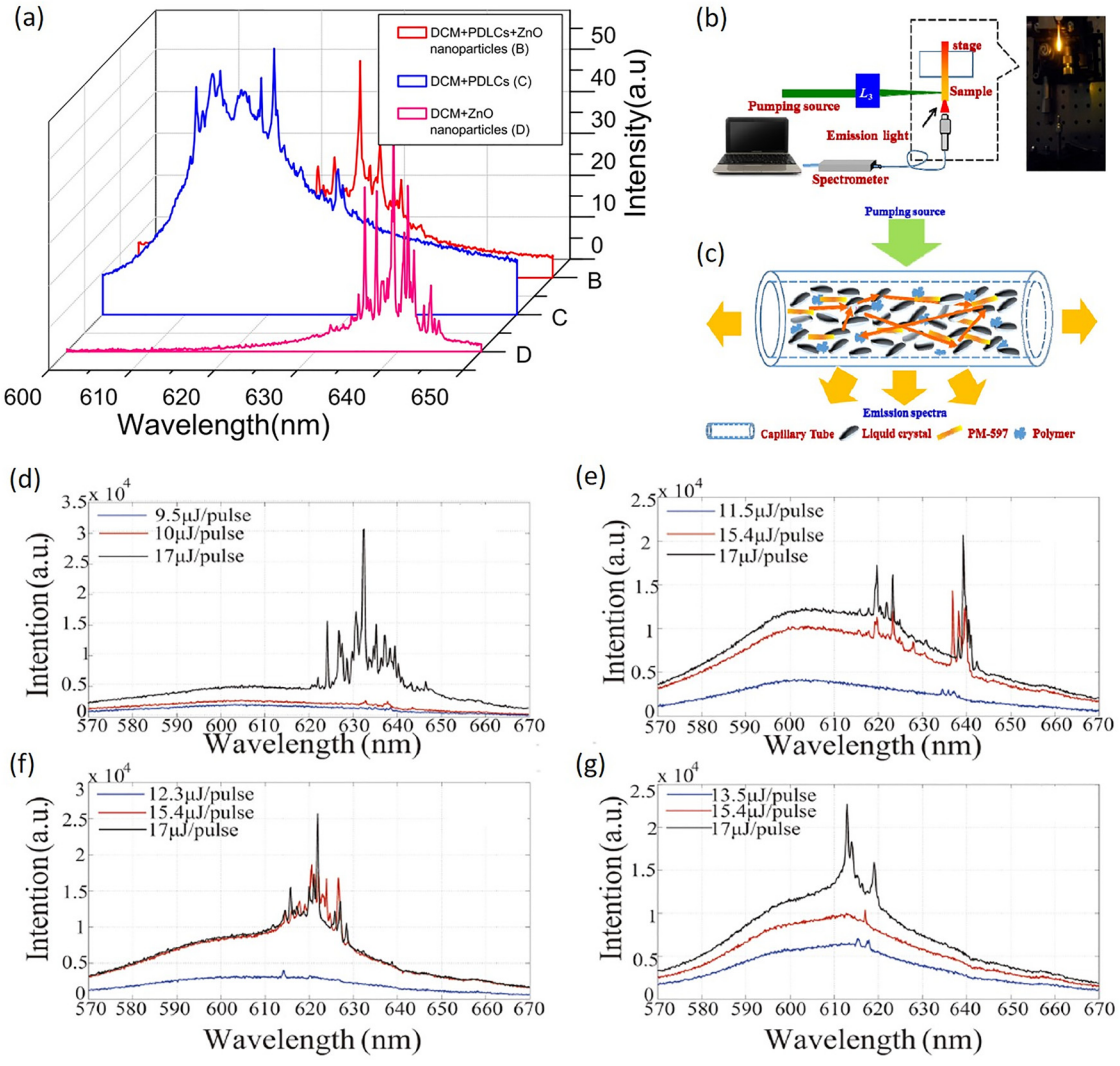

Figure 13: Emission spectra of DCM + PDLCs + ZnO nanoparticles (b), DCM + PDLCs, (c) and DCM + ZnO nanoparticles (d), respectively, excited by the pump energy above threshold [131] (a). Schematic illustration of the experimental setup of the random laser from the capillary tube infilling of the DD-PDLCs and photograph showed on the right (b), and the description of the multiple recurrent light scattering in the capillary tube comprised of the random alignment of LCs, monomer (NOA65), and laser dye (PM597) [132] (c). The spectra of random lasing from samples with MNP doping concentration of 0 wt.% (d), 0.01 wt.% (e), 0.02 wt.% (f), and 0.03 wt.% (g) in the PDLC with various pump energies [133].

indicates that metallic NPs always enhance light amplification phenomena independently of the used environment. Such an approach gave an insight into emission wavelength, RL energy threshold, and coherence of light modulation by the addition of ZnO nanoparticles. It originates from scatterers' permittivity and system geometrical structure [131].

Additionally, the approach concerning magnetic nanoparticles (MNPs) utilization in the working PDLC systems was also performed recently [133]. Dai et al. proposed a tunable random laser localized inside a tube, where the external magnetic field effectively influences the RL energy threshold, laser modes localization, and emission profile in general. Subsequently, it was proven that the magnetic field orientation tunes the light amplification in a meaningful way. The MNPs various concentration gave significant change in the output signal, what was experimentally proven (Figure 17(d–g)).

Ja-Hon and Ying-Li have presented a simple and effective DDPDLC random laser constructed in a capillary tube [132]. The idea of the experiment and the generated phenomenon with the proposed mechanism is shown in Figure 13(b). As it is visible from the sketch and the inset photo, the output emission was collected from the edge of the sample using a fiber spectrometer. The emission directionality is forced by liquid crystalline domains orientation as the response on the electric field coming from pump beam intensity and the internal reflection present inside internal curvature leading to waveguide phenomenon. However, the random lasing coherence and laser mode positioning can be easily tuned by polymer cluster shapes due to the various monomer concentration and morphological textures (grain size). The emission parameters, like FWHM, laser energy threshold, or a number of RL spikes from DDPDLC systems, can be easily changed, which was experimentally proved by the authors (Figure 14) [132].

As shown in Figure 14(a), the fluorescence band measured for PM597 laser dye is typically broad when a CW laser serves as the pump. Then, by stimulating the LC dye-doped sample without monomer, the emission band becomes narrower (down to FWHM ~11.4 nm). However, since the NOA65 monomer is gradually added, the discrete laser modes with FWHM equal to or lower than 1.0 nm start to arise and achieve the highest Q factor ~1135 and the lowest spectral broadness (0.52 nm). Above 20% of NOA65 concentration, the number of laser modes and their intensity decrease, especially those observed at 600 nm (red-shifted). It was explained that scattering losses started to dominate over optical gain.

Interestingly, the investigation also assumed spectroscopic experiments in the lower temperature conditions.

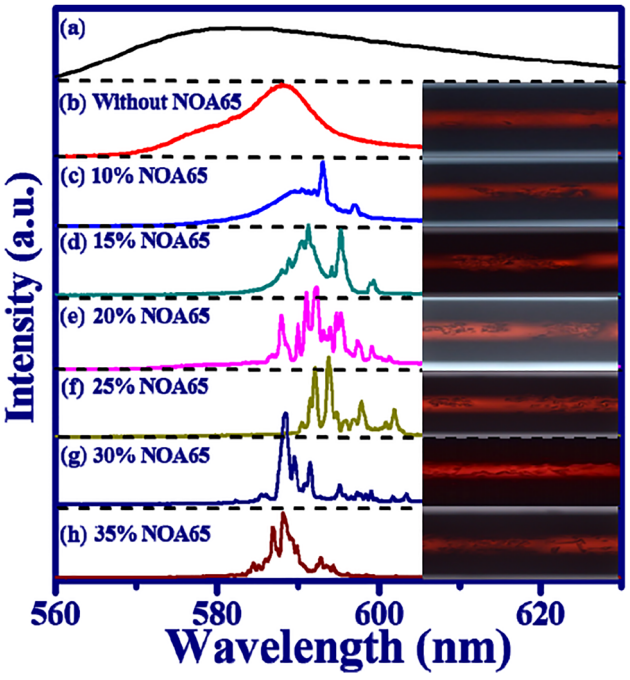

Figure 14: (a) The RT-PL of laser dye (PM597) and the RT stimulated emission spectra from the capillary tube through exciting the Q-switched laser that contains the DD-LC mixtures (b) without monomer and with (c) 10 wt.%, (d) 15 wt.%, (e) 20 wt.%, (f) 25 wt.%, (g) 35 wt.%, and (h) 35 wt.% monomer doping concentrations. The POM pictures of the DD-PDLCs are shown on the right of each diagram [132].

The investigated range of temperature was considered between 11 and 50 °C. Since the heat flow was supplied to the DDPDLC system, the emission nature began to transform from coherent random lasing to the ASE. The laser modes were suppressed due to the decrease of birefringence coming from the liquid crystalline domains with the higher temperatures. At around 11 °C, the LC-based system characterizes a much higher difference between ordinary and extraordinary refractive index than at 40 or 50 °C. Significant optical birefringence below room temperature for the considered DDPDLC system provides stronger light diffusion related to the more effective light scattering.

5.3 Quantum dots

Another family of LC-based random lasers is established on the utilization of quantum dots (QDs) as a luminescent dopant. Namely, in the systems where metallic QDs were applied due to surface plasmon resonance (SPR), the lower energy thresholds were acquired [134]. This kind of approach characterizes two main advantages. The first one comes from the NLC structure, where the applied external

electric field easily modulates emitted laser light intensity. On the other hand, the implemented QDs cause significant amplification of the generated light (Q factor increases) and decrease the energy threshold to obtain RL. Such a solution also has limitations related to the QDs concentration, which was shown in the literature by Ye et al. [134]. Too high quantum dots addition might quench light amplification and hurt the effective light diffusion. Also, the mutual arrangement between active molecules (dyes) and scatter units (QDs) is not trivial and always needs to be optimized during NLC random laser construction (Figure 15).

Also, a titanium nitride (TiN) was used to improve lasing action in the LC-based systems [120, 121]. Here, nanomaterials created plasmonic effects in the visible and near-infrared regions. The plasma frequency (ω_p) can be described as:

$$\omega_p = \left(\frac{4\pi n e^2}{m}\right)^{1/2}, \tag{5}$$

where n represents electron density in the material's volume; e and m are charge and electron mass, respectively [135]. For the higher carrier concentrations, the plasmon frequency can exist for the visible range of the spectrum. In comparison with noble metals, the TiN nanoparticles have significant advantages. For instance, their optical features can be modulated during the synthesis procedure environment. Then, the titanium nitride is compatible with the standard fabrication CMOS processing. Finally, the most important issue, TiN quantum dots, are much cheaper and can provide the same effect as the noble metals (Ag or Au). RL obtained from the NLC system doped with TiN NPs characterizes the FWHM parameter less than 0.3 nm for defined modes, which gives a Q factor ($\lambda/\Delta\lambda$) more than 2000 [136].

Moreover, if we compare RL with the PL spectrum, there is a significant red-shift by about 20 nm. This is caused by the increased dye re-absorption abilities by the TiN presence. The light amplification issue coming from the implemented nanoparticles to the active NLC sample comes from the localized SPR discussed before and the enhanced light diffusion, especially for the particular selected wavelength, which is in resonance.

Furthermore, the sample architecture significantly impacts the stimulated emission efficiency, as was shown

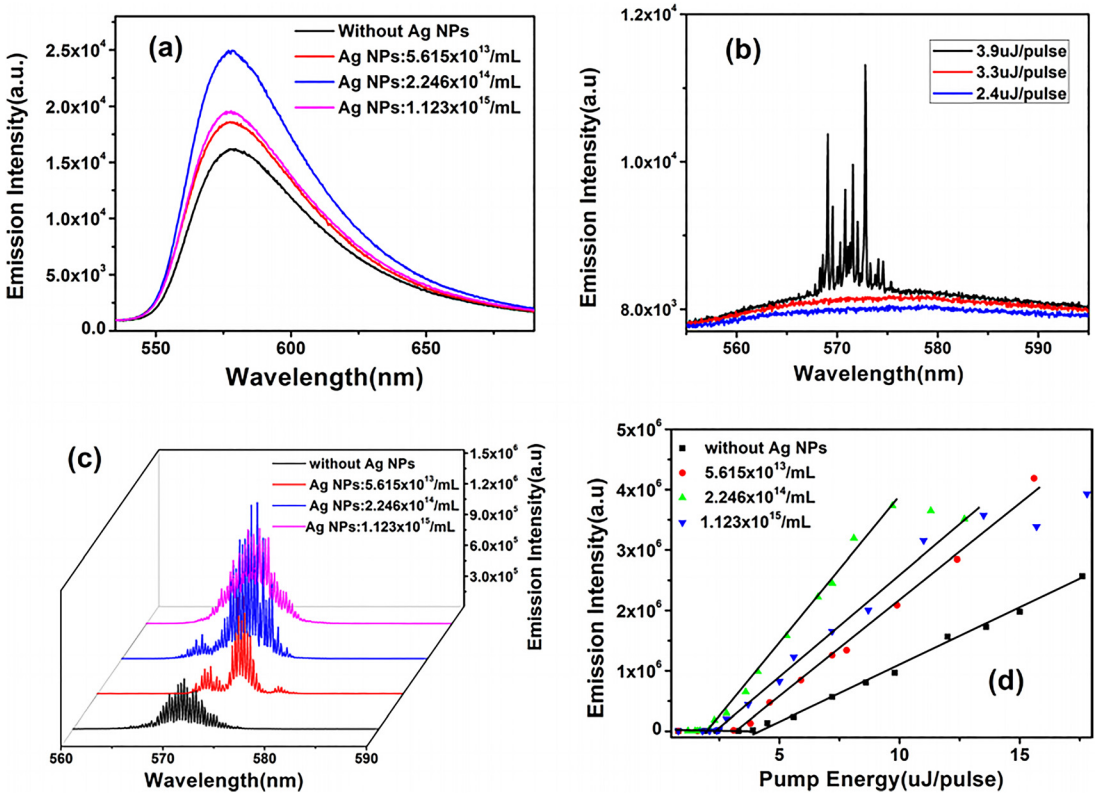

Figure 15: (a) Emission spectra of fluorescence from the toluene solution of PM597 laser dyes containing different Ag NP concentrations under the pump energy of 32.4 μJ/pulse. (b) Emission spectra as a function of pump energy for the NP-free DDNLC. (c) Emission spectra of RL from the NPDDNLC with different Ag NP concentrations under the pump energy of 7.2 μJ/pulse. (d) The threshold energy curves of RLs from the DDNLC with the addition of different Ag NP concentrations [134].

recently by Wan et al., when NLC-doped with TiN nanoparticles was placed in the capillary [136]. Interestingly, the emitted light intensity is related to the various directions from the active medium (Figure 16).

In the above example, it was found that maximum intensity was noticed in the long capillary direction when the pumping laser polarization is rotated in the same horizontal direction. There are a few possible mechanisms that indicate such a phenomenon. First, the capillary can be treated as a one-dimensional object, where the light diffusion takes place along the structure and is also reflected from the internal walls surrounding active material. Second, the light emission is related to the pump beam's polarization direction and dipole moment transition of the luminescent dye. For the same reason, the highest lasing intensity will be along the capillary length when the initial laser polarization is parallel to that direction. The next reason is related to the gain coefficient, which is connected with the electric field enhancement by localized surface plasmon resonance of TiN NPs, which is mainly present along the initial laser light polarization direction. Lastly, thanks to the line-shape pumping irradiation on the sample, the other emitting directions are not favored due to geometrical reasons [136].

5.4 Semiconductor

Semi-conductivity can be realized differently, in various types of materials, like π-conjugated polymers, nanoparticles, or quantum dots. In the organic systems, the maximum value of the valence band is replaced by the highest occupied molecular orbital (HOMO) π-type. Whereas the minimum value of the conduction band is represented by the lowest unoccupied molecular orbital (LUMO) π^*-type [137]. Between these two energy levels, an electronic bandgap is localized. The most practical advantage related to organic-based structures is the almost

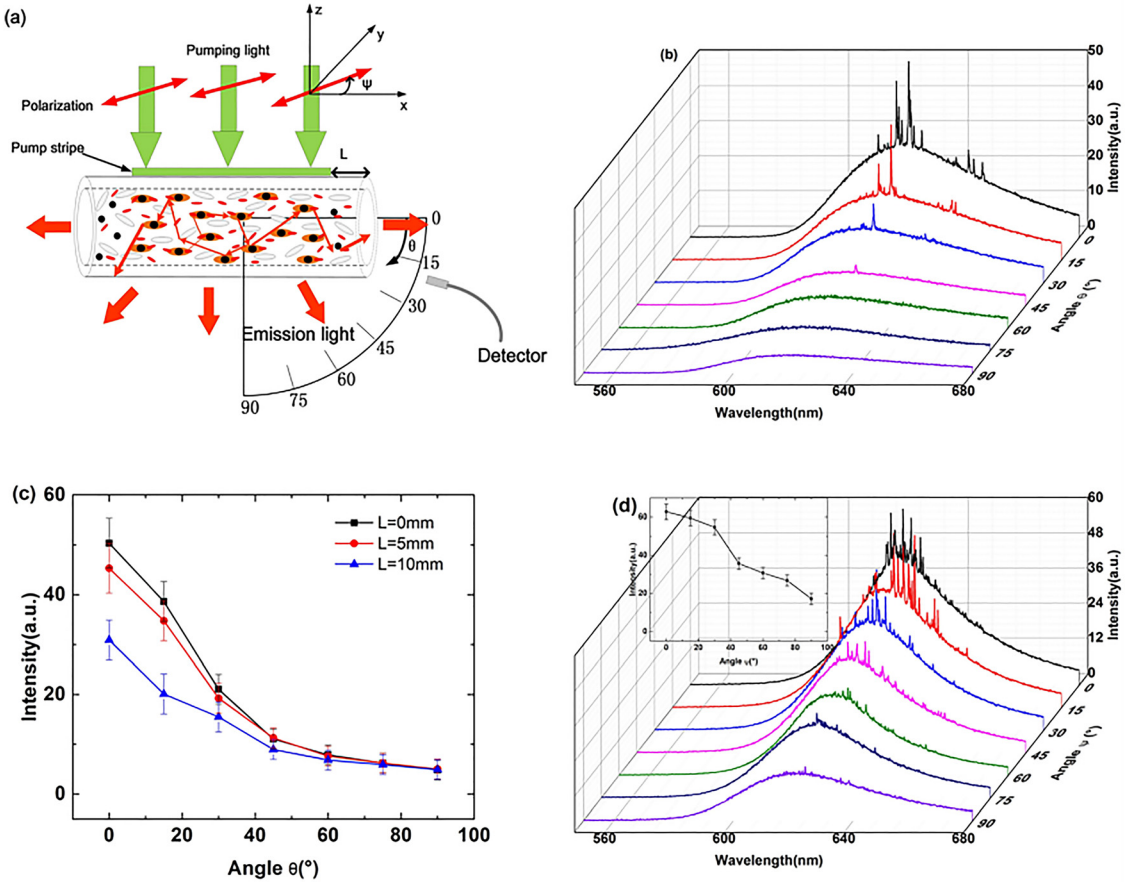

Figure 16: (a) A schematic illustration of the emission spectrum is detected at different angles. (b) The emission spectrum detected at different angle θ from the NPDDNLC sample with 1.186 × 1011/ml in TiN NPs number density, when L = 0 mm, ψ = 0°. (c) The peak intensity of the emission spectrum as a function of the angle θ, when L = 0, 5, and 10 mm. (d) The emission spectrum of the NPDDNLC sample with 5.314 × 1011/ml in TiN NPs number density as a function of the polarization direction ψ of the pump beam, when L = 0 mm, θ = 0°. The inset in Figure 22(d) shows the peak intensity of the emission spectrum as a function of the angle ψ, when L = 0 mm, θ = 0° [138].

unlimited possibility of designing and creating various molecular architectures, which is also easily implemented in photonic devices [4, 102, 107, 138]. Organic semiconductors found many applications not only in the organic light-emitting diodes (oLEDs), solar cells, or field-effect transistors (FETs) but also in the random laser constructions [137]. Random laser intensity can be easily controlled by the different exposure times of the constant-wave laser influence, in green or red (Figure 17(a)). The initial laser beam (in the pulsed working regime) generates the optical gain; the other cw ones control LC phase transition (nematic/isotropic). Consequently, refractive index changes influence the scattering level. Thus, the output power is modulated efficiently.

ZnO [140] or CdS [141] semi-conductor nanoparticles can serve as examples of their use in LC-based random lasers. Such constructed devices might be easily modulated when concerning their working parameters, like output wavelength or current threshold, making them appealing applications. The origin of such a possibility given by nanoparticles comes from their thermal and electrical stability. Moreover, since the NPs concentration increases, the number of scattering centers is higher; the emission wavelength is red-shifted according to the effective refractive index value changes in the considered disordered systems [141]. In summary, the most significant advantage of the semi-conductor NPs combined with LC is an increase of the light absorption, and secondly, more effective (up to 85%) photon delivery to the active medium.

The next approach to improve LC-based random lasers is to utilize quantum dots [142]. Despite the lowering of the energy threshold, a significant increase in the system's photostability constitutes another advantage. Wang and co-workers have proven high RL stability even after 15 days of laser pumping (approximately 3 h/day), which was estimated to be around 92% of the initial output laser intensity [142]. Nevertheless, another report [139] pointed out that even QDs additives can be insufficient without an LC matrix. The critical issue is to control the liquid crystalline phase transition related to the environment temperature. When the LC goes to the isotropic phase, the light-scattering ability of the considered system dramatically decreases, which results in emission band broadening and intensity decreasing (Figure 17(c)). In other words, LCs play a pivotal role in disordered media dedicated to the random lasing phenomena. However, the predominance of QDs under the NPs is significant. They provide a broader absorption band, the higher photoluminescence quantum yields, and give luminescence, where the output wavelength is easily controlled by synthesis duration and temperature.

5.5 Perovskites

3D Perovskites, nanoparticles, and nanoplates create a natural resonance cavity, which serves to achieve the population inversion needed for amplified spontaneous emission or lasing action [143]. Thanks to the wide modulation range of bandpass in Perovskite-based lasers, it allows their utilization in many kinds of applications, which will be described in this review. Imposingly, such constructed organic-inorganic systems achieved the same efficiency and brightness in two years, whereas organic LEDs technology has improved these parameters in two decades [143]. The first demonstrated device achieved effective biomolecular recombination by spatial electron and holes closing in the thin active layer (~15 nm). In that way, low exciton Perovskite energy is overpassed [143].

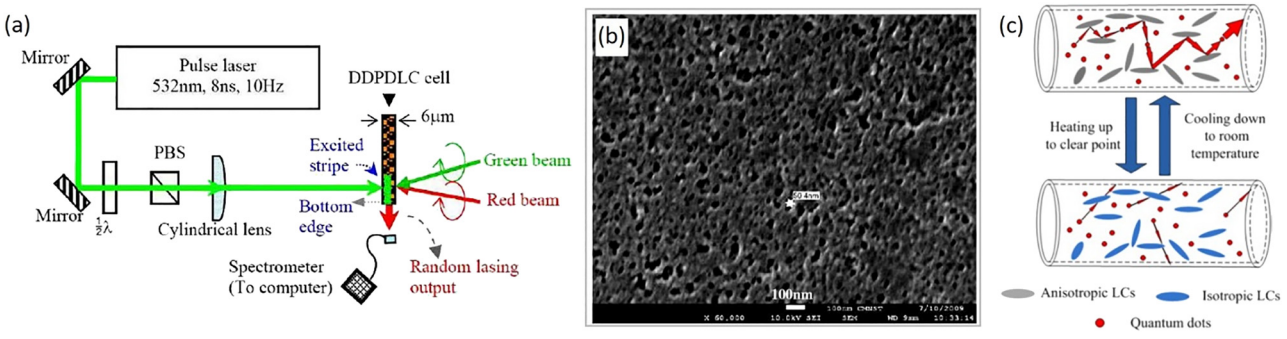

Figure 17: Top view of the experimental setup for examining the all-optically controllable random lasing emission of the DDPDLC cell (6 μm thick). The green and red beams are circularly polarized (λ/2, half waveplate for 532 nm; PBS, polarizing beam splitter) (a). The SEM photograph of the DDPDLC cell, in which the length of the white bar is 100 nm, and the black regions are places occupied by nano-sized LC droplets in the polymer matrix (grey regions) [137] (b). Schematic diagram of light propagating in the QD-PDLCs with LCs in the anisotropic phase and the isotropic phase [139] (c).

In 2015, Stranks et al. presented enhanced ASE based on the cholesteric LCs, where Perovskites were also applied [144]. The authors improved the mirror-less LC-based system so far that it could achieve single-mode and flexible laser structures.

In the above-cited contribution, the LC layer was deposited by spin-coating technique on the previously rubbed substrate (polyimide glass plate) (Figure 18(a)). Thanks to the transparent and reflective range of the liquid crystalline layer, it was feasible to combine $CH_3NH_3PbI_3$ Perovskite active medium to be the most effective. Moreover, for the same reason, additional sandwich-like spacer layers were applied (SEM cross-sectional photo is presented in Figure 18(b)). Interestingly, the authors noticed an unexpectedly strong light amplification and emission spectrum narrowing effect featured with the addition of CLC, which excludes superfluorescence or excitonic effects [145–147]. The effect was experimentally proven and shown in Figure 18(d). The authors postulated that only thanks to the CLC utilization, it was possible to decrease the energy threshold to observe single-mode RL on the mirrorless lasing systems lower (~7 μJ/cm^2/pulse) than already presented in the literature [148, 149]. Then, also wavelength tunability and whole architecture flexibility are provided by CLC as the reflector to the demonstrated organic-inorganic systems (Figure 19(a)).

Wenzhao et al. have presented Perovskite microdisk lasers doped with 5CB liquid crystal, where the output signal was easily tuned and switched by environmental temperature changes [150]. The authors found two types of RL tunability: a small type (~1 nm) due to the LC refractive index changes and a much larger type (~6 nm) related to the scattering media modulation. In the just-cited contribution, the authors showed an LC-based Perovskite-type nanolaser, based on the nanowire-shaped active medium embedded in a well-aligned environment (Figure 19(b) and

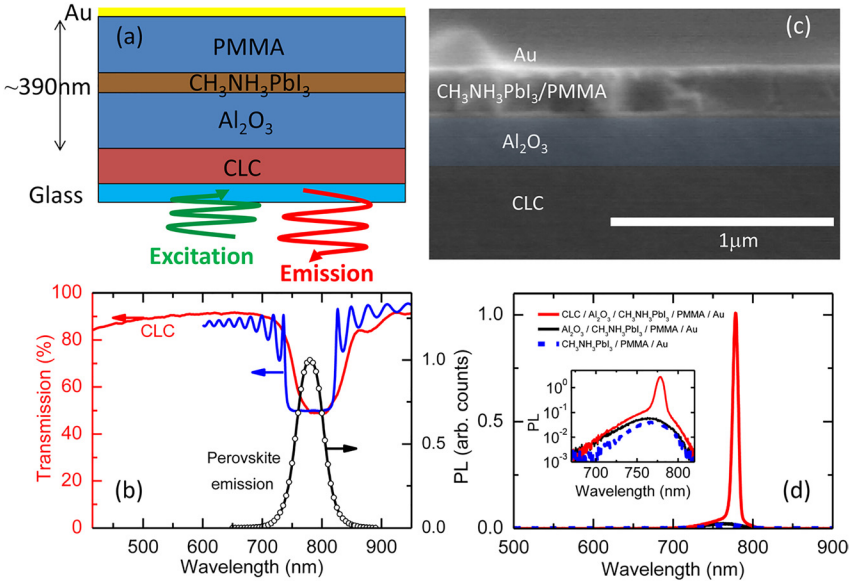

Figure 18: (a) Schematic of the device stack. (b) The transmission spectrum of the CLC reflector on glass (left axis) with PL spectrum from the perovskite thin-film overlaid (black circles, right axis). The blue line shows the modeled transmission spectrum of the device stack using the 4 × 4 Berreman matrix approach. (c) SEM cross-sectional image of the full device structure on the glass. The alumina layer has been shaded for contrast. (d) Emission from full device stack (red), stack without CLC (black), and stack without CLC and alumina (blue dashed), with pulsed excitation (530 nm, 4 ns pulses, 10-Hz repetition rate, ~60 μJ/cm^2/pulse) [144].

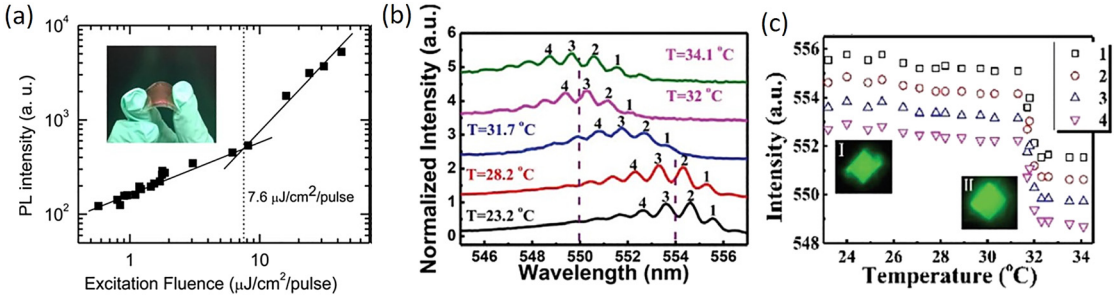

Figure 19: (a) Extracted emission intensity from a device stack fabricated on a flexible 80% CLC reflector following photoexcitation at a range of fluences (532 nm, 5 ns pulses, 100-Hz repetition rate). The ASE transition fluence is determined to be 7.6 μJ/cm^2/pulse. Inset: photograph of the flexible device [144]. (b) The laser spectra of liquid crystal-covered perovskite microdisks at different temperatures. (b) The peak positions of modes in (c) as a function of temperature. A dramatic wavelength shift can be observed at T = 32 °C [150].

(c)). The system was characterized, and at the same time, the output laser wavelength was tuned in the temperature range of 24–34 °C. The separated modes of a random laser were shifted by about 4 nm. This effect was explained by the scattering medium modulation being more efficient when external heat flow is provided and due to the unique LC features (transition from nematic up to the isotropic phase) [150].

Another proof of the obtained highly efficient (RL energy threshold ~150 nJ/pulse) and narrow linewidth effect (FWHM ~0.20 nm) in CLC-based laser with lead-free cesium tin halide (Perovskite) active material was recently given by Chen et al. [151]. Moreover, these authors reported a low-cost manufacturing method to achieve multicomponent Perovskite-based lasers. From the future applications point of view, the long spectral stability of the induced lasing action is the most important feature (Figure 20).

Also, Arumugam et al. have shown that thanks to the application CLC as the reflective layer, Al_2O_3 and P_3HT working as spacers, and finally, due to the active Perovskite medium ($C(NH_2)_3PbI_3$:Tm), it was possible to achieve a high *Q*-factor equal to ~2500 [152]. The CLC layer dramatically reduced emission bandwidth to 0.28 nm with a pump laser equal to 0.70 μJ/cm^2. These results paved the way for using Perovskite materials doped with LCs as efficient photovoltaic and electro-optic applications.

6 LC microlasers and other constructions

Liquid crystalline matter can be considered as a valuable component for developing different laser devices, similar to the random and band-edge constructions presented above. In this chapter, the focus will be given to liquid crystalline microlasing constructions known as Whispering Gallery Modes (WGM), plasmonic and biological LC microlasers, together with the discussion of their physical properties, modern and future applications.

6.1 Whispering gallery mode (WGM)

Whispering gallery mode (WGM) resonators are optical cavities in which light can be guided around and circulate, based on the phenomenon of total internal reflection. Such a situation takes place on the curved surfaces of the cavity. Therefore, WGM appears in a sphere or ring, and they are characterized by a higher refractive index value compared to the environment. The *Q* factor in such an example can reach the value of 10^{10}, which is considered a great advantage [153–157].

As the main configuration of LC supporting WGM operation, a liquid crystalline matrix with introduced luminescent dye is used, finally excited by the use of an external source of light. By embedding the cholesteric droplet into the water, the cavity can reach a size of about 30 μm diameter. Such a prepared microresonator enables the fabrication of liquid-phase exhibiting a very low lasing threshold. According to the reference, the resolution of the CLC microdroplet-based temperature sensor is 4.17×10^{-2} ° C. These constructions are perfect for integration in optoelectronic devices. It is now worth considering the sensor's applications, which can be achieved thanks to the small size and high *Q* factors. For example, WGM sensors can be made of cholesteric mesophase, known as sensitive for temperature changes (Figure 21(a) and (b)) [157].

An interesting aspect of operating WGMs microcavities is the possibility to tune the resonant frequencies (even in real-time) by changing different stimuli. One can be the optical path of the light, while the second acts on the resonator refractive index changes. It is also possible by varying the resonator physical dimensions. Among the major ways and stimuli influencing the mentioned factors, it is worth mentioning temperature, mechanical stress, and electric or

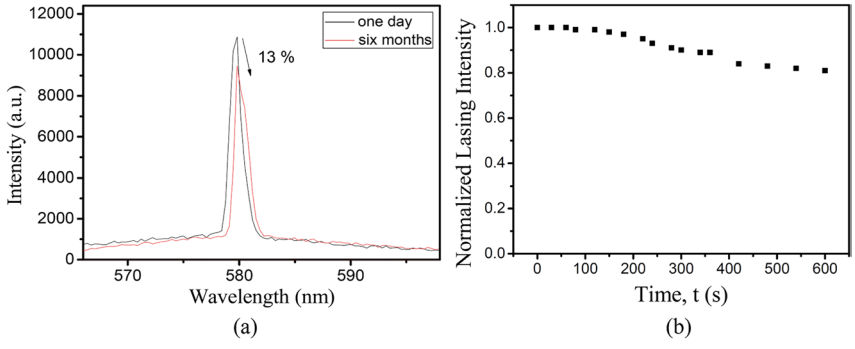

Figure 20: (a) Lasing spectra of the AIPQD–CLC (cell 1) at E = 0.6 μJ/pulse after 1 day and 6 months of storage (black and red peaks, respectively) under room temperature (23 °C) and high humidity of 60% (±5%). (b) Variation of the measured lasing intensity of the AIPQD–CLC device under continuing excitation of the pumped pulses for 10 min. The measurement was performed under room temperature (23 °C) and high humidity of 60% (±5%) [151].

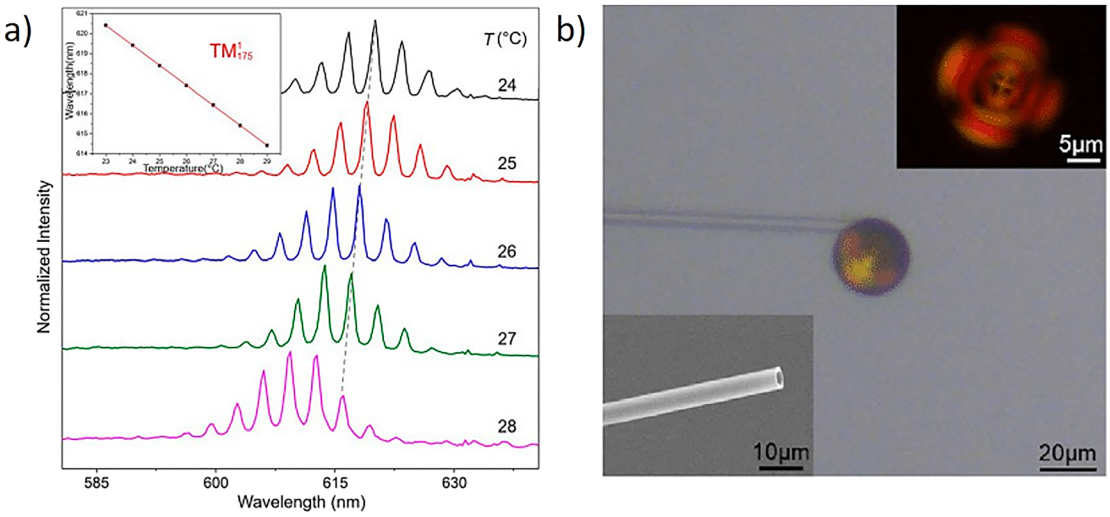

Figure 21: (a) Lasing spectrum of 22 μm CLC microdroplet as a function of temperature from 24 to 28 °C. Inset: temperature dependence of the lasing wavelengths of the representative mode TM_{175}. The wavelengths exhibited an almost linear relationship with temperature (0.95 nm/°C); (b) Micrograph of a 20 μm dye-doped CLC microdroplet confined at the tip of a capillary microtube. Insets: close-up POM image of the microdroplet (upside); SEM image of the microtube (underside) [157].

magnetic fields [158]. The effects have been referred to in the literature as obtained on ferronematic LCs. The investigated liquid crystalline nematic mesophase is named 6CHBT (1-(trans-4-Hexylcyclohexyl)-4-isothiocyanatobenzene) doped with spherical or rod-like magnetic particles (Figure 22). The results present the shift towards red under the influence of the magnetic field. Moreover, the sensor's measured sensitivity was increased by changing the WGM diameter size (from –39.6 pm/mT and –37.3 pm/mT to –61.86 pm/mT and –49.88 pm/mT for rod-like and spherical magnetic dopants, respectively).

LC microlasers working as WGMs can also be realized for the nematic mixtures, for example, E7. Moreover, they can be easily tuned by an external magnetic field. When the applied field is considered as in-plane geometry of the WGM circulation, the lasing modes shift towards the blue. However, perpendicular to the circulation plan of WGM, the spectrum shifts towards red. Almost the same magnitude characterizes both cases, and the effect is fully reversible [159].

The electric field tuning in the LC matter is especially interesting since it is usually fast and can be easily integrated into, for example, current electro-optical circuits [156].

It is worth recalling the LC-based constructions combined with polymers. Embedded in the polymer, matrix LC-dye-doped droplets from the phase-separated microcavities make lasing possible. These kinds of devices have been created and are still developed as previously described PDLCs. To achieve this construction, the proper methods for homogenization must be applied, such as the use of ultrasounds or the evaporation of used matrix solvents. The main advantage of PDLCs is the possibility to create the required and expected microresonator size [160]. Liquid crystalline droplets embedded in a polymer matrix remain in the

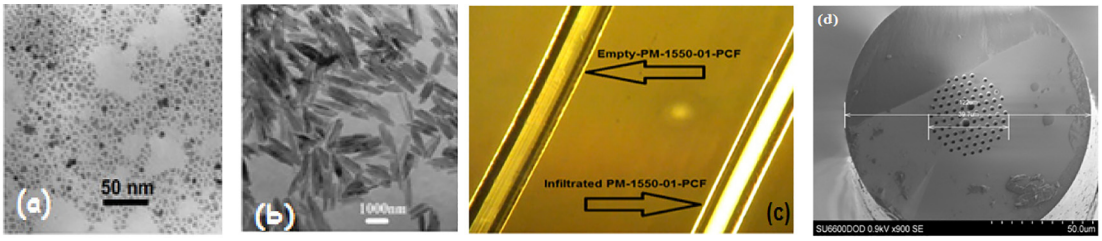

Figure 22: TEM images of (a) spherical magnetic nanoparticles, (b) rod-like magnetic nanoparticles, (c) polarizing microscope images of empty and infiltrated PCF in crossed polarizers, and (d) SEM image of the PM-1550- 01-PCF cross-section [158].

droplet-shape and, therefore, can be interesting for the WGM applications, size modulations, and lasing performance. An advantage of these devices is that they allow for the investigation of more than one luminescent dye dopant. With the mix of three luminescent dyes emitting in the fundamental colors (green, blue, red), it is possible to obtain a white-lasing device, which can be easily tuned by the applied external fields [103].

6.2 Plasmonic

Another approach involves plasmon-associated issues. Plasmon-based lasers have many advantages, including ultra-compact, small sizes reflecting in easy integration in optoelectronic devices, low threshold, generation of coherent light in nanometer-scale beyond the limit of diffraction, short response time, and light localization providing the strong and efficient output [161]. It is worth noting the remarkable tunability and sensing properties of LC mesophases. Surface plasmon-LC combined systems can find application in QDs laser devices or optical planar circuits switches [162]. It can be realized via the Tamm-Plasmon Mode, formed between a metal and dielectric Bragg mirror. Therefore, it can be connected with the photonic crystal substrates. The presented method bases on the preparation of a small LC gap layer (in the range of 200 nm), placed between the photonic crystals and metal surfaces (Figure 23(a)).

By changing the temperature of LC, affecting phase evolution (between isotropic and nematic), it is possible to obtain different resonance wavelengths (a shift about 15 nm). Combining the LC mesophase with the plasmon technologies is very interesting for future, novel display ideas [164]. With the investigation of LC-display technologies, the aluminum plasmonic nanostructures can provide low cost, good quality colors, and resistant to fast bleaching. Such technology could be combined with the idea of novel displays pumped by the laser source (e.g., UV range), ensuring an excellent quality color gamut and easy tunability. Surface plasmons (SPs) can be combined with LC mesophase and metallic nanoparticles [165] in the form of micro, PDLC droplets. The evidence of plasmonic excitation in this context leads to the further possibility of creating plasmon-LC-hybrid lasing devices for coherent, efficient, directional, intense lasing from well-defined microresonators. Chiral liquid crystalline molecules (CLCs) are well known for the existence of the photonic bandgap in their structure. The novel studies conclude that CLCs doped with gain medium and gold nanoparticles can strongly enhance the fluorescence signal via localized surface plasmon effect [163]. For referred studies, the defect of the investigated layer was prepared by the use of commercially available materials, like an E7 mixture doped with pyrromethene (PM597) laser dye. The effect of enhanced fluorescence is presented in Figure 23(b).

The photonic crystal characteristic of dye-doped CLCs is very promising for further studies of Surface-Plasmon lasing under the influence of electric, magnetic field-tuning, or mechanical stress.

Another example of tunable nanophotonic structures formed by LC and metallic nanostructures (based on spherical, gold nanodots, nanodiscs, nanorods) is localized surface plasmon resonance (LSPR). LSPR is a particular type of SPs, occurring with the use of nanoparticles. The LSPR is observed when the electromagnetic field remains localized in a nanoscale region around the nanoparticle-dielectric interface [166]. These constructions are very appealing for novel tunable devices, like LC-based displays, light emitters, and biosensors, which will be discussed in the next section of this chapter [148, 167].

6.3 Biological

In the context of biological applications, it is worth recalling the WGM resonators, which can easily interact with the environment. When the particle or even the single-molecule

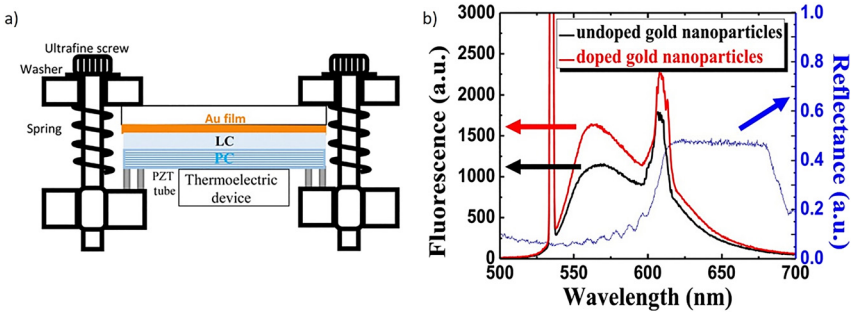

Figure 23: (a) An apparatus for changing the LC gap by using fine screws and PZT tubes [147]; (b) Stopband reflection of CLCs (blue curve) and fluorescence spectra for undoped (black curve) and nano gold-doped (red curve) CLCs excited by a CW 532-nm laser [163].

settles on the WGM ring or can be found near its surface, the optical path of light, likewise the loss factor, changes significantly, and the object can be detected [168]. As mentioned before, a high *Q*-factor is a reason for the great sensitivity of these devices. Therefore, in the context of liquid crystalline microlasers, they became precious tools for detecting lipids [169], responses for pH variations [170], viruses, or proteins [171].

Here we cite an interesting example of a WGMLC-based resonator [172]. As with the LC mesophase, it has become a very popular and widely reported nematic liquid crystal, named 5CB (full name: 4-cyano-4′-pentylbiphenyl), doped with PBA (4′-pentyl-biphenyl-4-carboxylic acid) in a buffer solution (PBS). The first great advantage is selecting materials that are widely available, well tested, easy to use, and relatively cheap. The authors present the lasing signal and the droplet configuration for the pH changes (Figure 24).

Such an example can be considered valuable in oceanography, clinical, or environmental studies.

One of the latest discoveries shows that LC microdroplets can be useful in detecting negatively charged biomolecules [173]. This result opens new possibilities for ultra-sensitive bio-sensing in the scope of LC matter for novel diagnosis and biomedical science.

The LC microlasers are especially promising in the context of environmental monitoring, industrial drain control, drinking water quality testing, and waste treatment according to the possibility of heavy metal toxic ions detection [174]. For these effects, researchers have employed a commercially-available 5CB-nematic LC mesophase doped with stearic acid in the form of WGM microdroplets (Figure 25), thus forming a biosensor.

The sensing properties could be achieved according to the heavy metal ions adsorption, monitored by polarized pattern evolution, the observation of resonance shift, and spectral response. Because of the many tests and repetitions made on this device, this biosensor can be considered reliable.

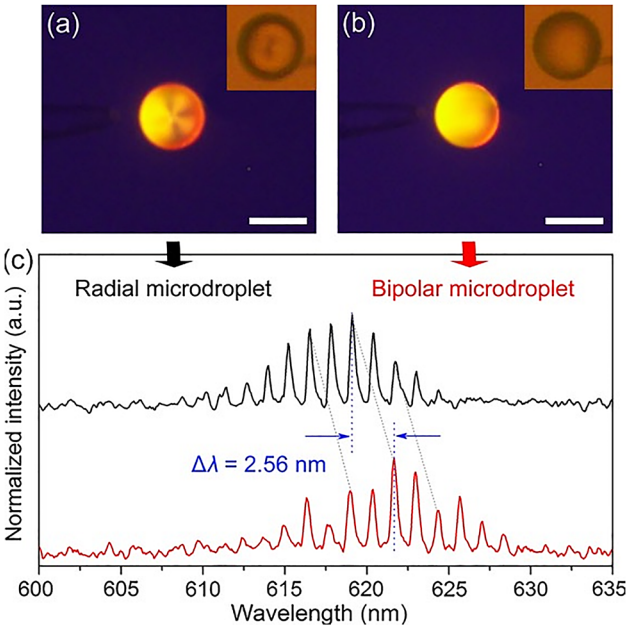

Figure 24: (a) POM image of lasing PBA-doped 5CB microdroplet in PBS with a pH of 6.0. The microdroplet exhibits a radial configuration. The corresponding micrograph of the radial microdroplet (top right inset). (b) POM image of the same microdroplet 3 min after adding 10 µL hydrochloric acid solution: the microdroplet undergoes ordering transition from radial to the bipolar configuration as the pH decreases. Scale bars 50 µm. (c) WGM lasing spectra of PBA-doped 5CB microdroplet with radial (black line) and bipolar (red line) configurations [175].

7 Applications

7.1 Sensors

Since the heat sensitivity is a typical property for the NLC, these can be used as remote thermal sensors, where by using a telescope, the response signal can be analyzed [118]. Because of the synergic effect of the NPs and QDs combination, it was possible to achieve polymeric fiber optic random lasers, sensors, and displays [142]. The LC-based sensor, recently proposed by Duan et al., has a great sensitivity to urine molecules and can detect a molecular concentration as low as 0.1 mM [175]. That system has many advantages. Namely, quantitative and sensitive detection takes place in real-time processing, and its resolution (detection limit) is much higher than previously described urea detectors. These advantages are a result of the acid-doped 5CB liquid crystal and WGM lasing technology. It revealed in a dual light amplification and emission band shift, which comes from LC microdroplets configuration transition. This feature makes such systems excellent candidates for monitoring enzymatic reactions (Figure 26).

There are many more examples of such applications. For instance, LC-based sensors were introduced to detect various biological molecules (i.e., lipids [176], glucose [177], proteins [178]), but also heavy-metal ions [179, 180] or synthetic polymers [179]. Then, using the synergetic effect of the up-conversion nanoparticles (UCNPs) and cellulose LC, it was possible to construct a real microfiber humidity (RH) sensor (Figure 27) [181]. The mirrorless low threshold lasing provided by the LC-based part, together with UCNPs fluorescence molecules, provides a highly sensitive RH detector

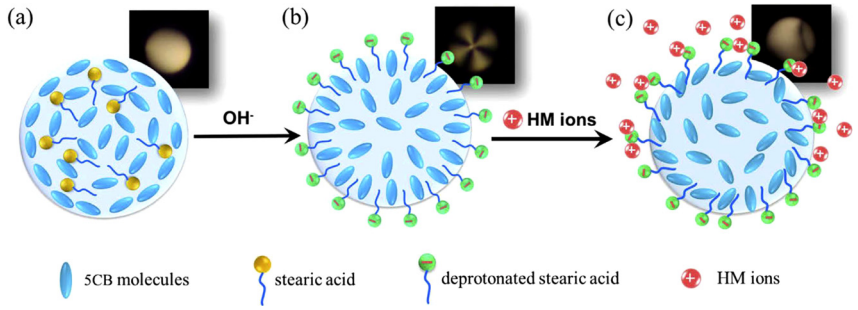

Figure 25: Schematic illustration of the orientational transition of stearic acid-doped 5CB microdroplets induced by changes of 5CB anchoring at the LC/aqueous solution interface.
(a) without HM ions at pH = 6.5; (b) without HM ions at pH = 8.5; and (c) with HM ions at pH = 8.5 [174].

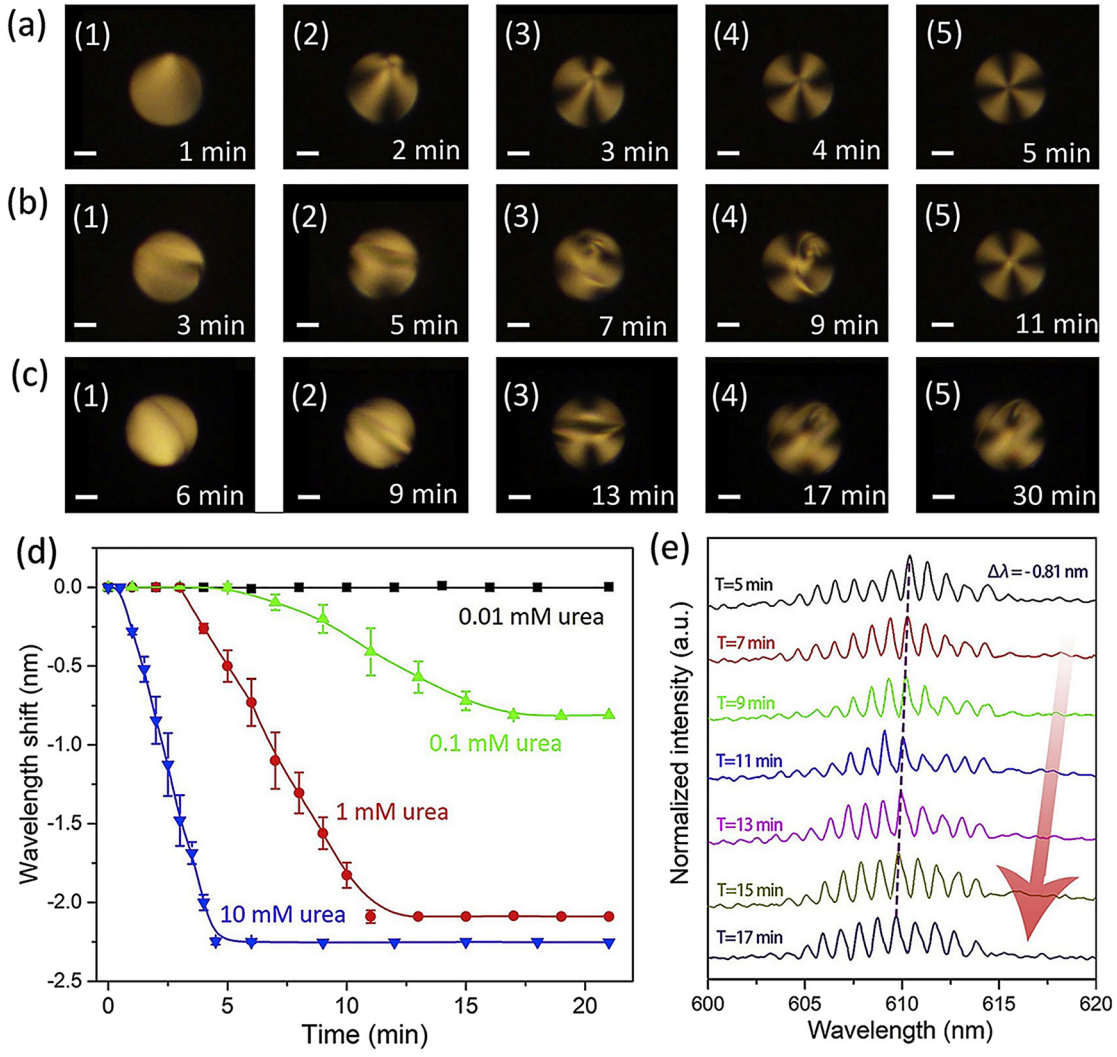

Figure 26: POM images of 65-μm-diameter acid-doped 5CB microdroplets in PBS (pH = 7) containing 0.1 mg/ml urease after addition of 40 μL of 10 mM (a), 1 mM (b), 0.1 mM (c) urea. Scale bars 20 μm. (d) Temporal dependence of WGM wavelength shift with different urea concentrations. (e) Portion of WGM lasing spectra as a function of time. Spectra were collected from a 65-μm-diameter acid-doped 5CB microdroplet in PBS containing 0.1 mg/ml urease after adding 40 μL 0.1 mM urea [175].

(284.75 pm/%RH independently of the environment temperature), which is shown in Figure 27.

The biosensor for heavy metals (HM) detection based on the LCs, which gives various lasing behavior, was recently introduced in the literature [174]. Again, the WGM mechanism was implemented to achieve a significant signal in the LC microdroplet sensor. The results indicate the discussed device as pioneering among currently known

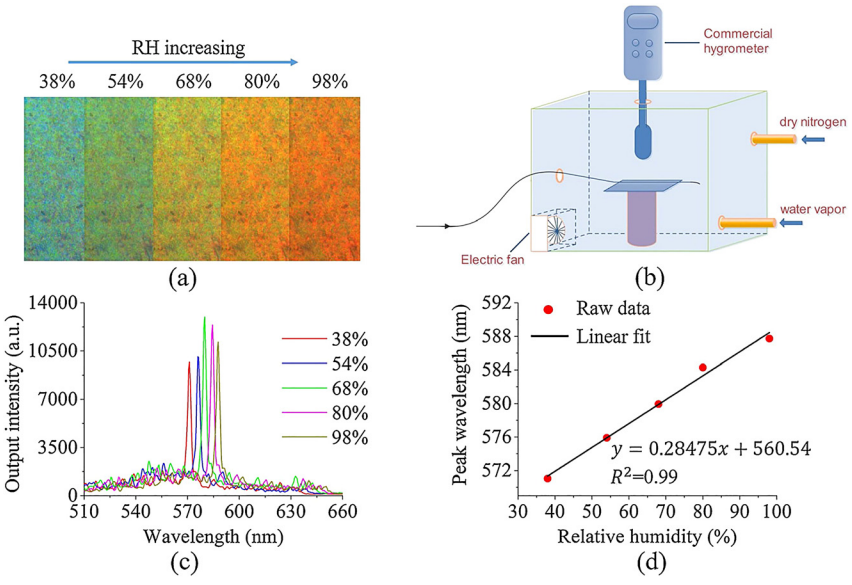

Figure 27: (a) ×20 micrographs of the planar CLC film at different RH levels. (b) Schematic diagram of the experimental setup for RH testing. (c) and (d) show the output spectra and the laser emission wavelengths at RH levels of 38, 54, 68, 80, and 98% [181].

systems dedicated to the detection of the HM ions. It was experimentally proven that the achieved sensitivity level is equal to 40 pM for Cu^{2+} ions, which is six orders of magnitude better (concentration threshold, when copper ions are detected) than that defined by the World Health Organization (WHO). Notably, the WGM LC-based sensor is selective as well when the light metal ions are considered, which helps to avoid any artificial signals. That example can be straightforwardly utilized to analyze drink water quality, or in general, to monitor the environmental condition (Figure 28).

7.2 Display technology

Due to the possibility of molecular re-arrangement in NLC random lasers using the external electric field, they started to be implemented in modern type LC displays (LCDs) [118, 182]. By adjusting the NPs concentration, which is embedded in LC-based laser displays, it is feasible to modulate the generated screen brightness [140]. LC-established random lasers doped with CdS semiconductor nanoparticles can be implemented as the optical element into the photonic structures or utilized in the holographic displays [141].

A full-color LC-based laser display was recently shown [183]. The adopted idea was based on inkjet technology, which leads to the construction of a flat-panel, micro-templated pixelated laser array. Single-mode RGB LC-based arrays were highly ordered on the well-defined microtemplates. In this way, the self-emissive panels provided a full-color laser (Figure 29). These results paved the way for constructing the other LC-based light sources, covering the full range of the visible spectrum.

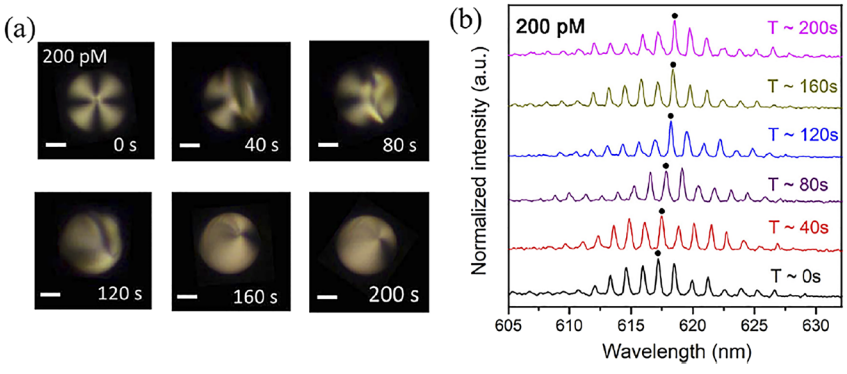

Figure 28: (a) Evolution of the POM images of stearic acid-doped 5CB microdroplets incubated with 200 pM copper(II) chloride in PBS solution (pH = 8.5). Scale bar = 20 μm. (b) Lasing spectra of stearic acid-doped 5CB microdroplet incubated with 200 pM copper(II) chloride in PBS solution (pH = 8.5) as a function of time. Black dots indicate the position of the WGM selected to monitor the spectral shifting of the droplet lasing emission [174].

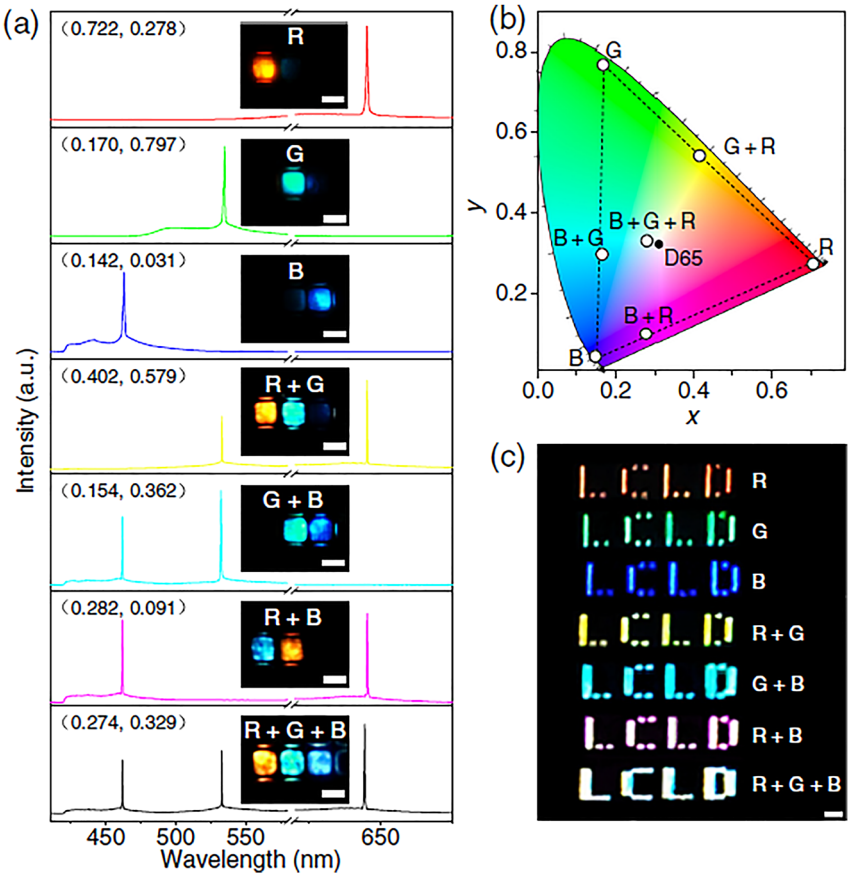

Figure 29: Full-color lasing combinations from RGB subpixels. (a) Lasing spectra of different combinations of RGB subpixels. Insets: Corresponding PL images and CIE1931 coordinates calculated from respective spectra. Scale bars = 20 μm. (b) Chromaticity distribution of the lasing peaks on the CIE1931 color diagram. The peaks were extracted from seven spectra in (a). (c) Far-field photograph of the "LCLD" patterns composed of different RGB pixel arrays. The photograph was captured by a built-in digital camera in a cell phone. The scale bar is 150 μm [183].

7.3 Others

Due to the high flexibility of the NLC-based random lasers, they can be utilized as flexible displays or in various military applications, such as identifying friendly or enemy units [144]. Thanks to the NPs utilization, LC-based random lasers can be applied as the new light sources and optical communication technologies [140]. Whispering gallery mode texture based on the liquid crystal can serve as an electrically tunable microresonator [184]. It has been proven [185] that liquid crystal cells can work as dynamic write-and-read media, thanks to the opportunity to create a diffraction pattern. Such a device can be easily adopted as an optically addressed spatial light modulator in technology's commonly known multimedia field. LC-based random lasers also have applications in spectroscopy and medicine [4]. Finally, a white laser based on the nematic LC was proposed very recently [103]. Interestingly, the presented NLC-based white random lasing intensity was also controlled by low external electric field application values. A temperature-controlled LC-based random laser was recently introduced by Wiersma and coworkers [186]. Such a device can be easily introduced for remote control sensing and in temperature-dependent displays or screens. The report given by W. Huang and coworkers paved the way for using LCs in distributed feedback lasers [82].

Supplementarily, the nematic LCs offer interesting applications in nonlinear optics [187]. DDNLC can also interact as the NLO medium in the manner of passive response (beam self-focusing and self-trapping), similar to the Kerr-medium in all-optical switching [188] phenomena. It can act together efficiently with the active part of the system (optical gain system) and, in this way, impart many advantages (e.g., all-optical control in the disordered systems generating single- and multimode random lasing). NLO-induced light sources or processors can be constructed based on the LC materials as well [188].

Lastly, information encryption and decryption have become alternative fields for the application of NLC [118].

8 Perspectives and conclusions

There has been noticed a rapid development of liquid crystalline lasing devices in recent years. Here we have

described the diversity of LC mesophases (e.g., cholesteric, nematic, or blue phases [39, 41]) and the many interesting ideas for their use in the context of light amplification. These factors make this research area outstanding and significantly emerging.

The different LC mesophases and their unique properties were used for implementing the idea of band-edge lasing [49] dedicated to the future ultimate light source manufacturing [189]. Interestingly, ideas standing behind the preparation of LC-dye hybrid systems have been proposed by academics and realized in the industry. This approach opens many possibilities for the use of modern and newly developed chromophores offering valuable properties for band-edge lasing, like BODIPY-dyes [50]. It is important to underline that this group of dyes is synthesized, functionalized, and examined so that they can be used in lasing technologies according to their excellent thermal- and photostability [50]. For instance, one of the main goals for modern optoelectronic technologies is to produce stable, efficient OLED- and WOLED-based devices (dedicated to progressive and improved TV screens, monitors, projectors, displays, and novel lighting technologies, such as Li-Fi). For this purpose, new hybrid materials, like LCs, are eagerly tested. These allow the construction of various systems, which can be formed as thin layers, LC cells, or microdroplets.

Moreover, they can be modularly introduced into other organic and inorganic materials (e.g., polymers and elastomers [47]) and whole, working devices [60]. Exploring the new active hybrid systems allows for the optimization of lasing properties and helps to combine them with already known devices to develop applications, such as biochemical labels, fluorescent switches, and sensors [190]. LCs are very useful and susceptible to structural, thermal, and optical tunability and assembling into 3D structures, making them well-suited to medical and biology applications. They can form systems with QDs, offering combined advantages typical for both types of materials, such as flexibility, sensitivity, and high photostability. The electrical control of LC mesophases facilitates the use of these materials to produce wide-broadband lasing devices, which can self-restore and rapidly respond to environmental changes.

Once again, it is worth noting the unusual LC structures, like Blue Phases, known for their improved temporal response of LCD. It will be important for the future to have an insight into the particular types of LCs that can distinguish tunability and excellent lasing emission properties [65], made possible through novel, ultra-fast light modulators, high definition displays, or tunable photonic crystals [191].

DFB lasers, according to their excellent sensing ability, relatively high power of the emitted light, and easy way to produce, are interesting devices for the incorporation of novel techniques and future improvements. Most likely, for this reason, the new ideas still appear in the articles and commercial use, for example, as modern DFB-LC hybrid systems. The method is based on photopolymerization or nanoimprinting UV technology, producing tunable devices and reliable sensors, which can be miniaturized [192]. Sensing properties, the possibility of precise layer thickness control, together with the ability to emit three basic colors simultaneously, are also worth mentioning in the context of developing surface-emission junction lasers (e.g., PSCLC and VCSEL). The possible prospects for these constructions include laser printers, lidars, and 3D sensors, among others.

Many scientists from various research groups have investigated the random lasing phenomenon. This kind of technology has been proven to lead to the construction of modern devices dedicated to lighting applications (Li-Fi concept), identification systems, bio-sensing, medicine, diagnosis, and laser-based displaying. RL achieved with nematic LC mesophase is characterized by easy tunability induced by the heat flow [88], electric, or magnetic fields. The obtained RL emission is efficient and possible for easy tuning – in the case of LCs, also by externally applied fields (magnetic/electric), mechanical stress, or temperature. Moreover, by exploiting different LC materials (e.g., cholesteric mesophase), it is possible to achieve the ultra-low RL threshold. The prospects for RL include lighting, imaging, fluorescence microscopy, creation of novel technology laser displays, biological sensing, chemical monitoring, identification, and communication [186]. Another referred lasing mechanism can be realized by the use of LC combined with QDs. In this case, the SPR phenomenon can be observed, which takes part in a significant reduction of the lasing threshold [134]. It is worth noting the very attractive Perovskite materials used for lasing in the form of 3D and different nanostructures (e.g., nanoplates, nanoparticles). In this case, it is worth mentioning the possibility to obtain very efficient amplification of light, accompanied by the narrowing of the obtained spectrum pointing to the one-mode RL phenomenon [145–147].

The next group of LC lasers, which are highly attractive to discuss, are PDLC microlasers. It is worth distinguishing future applications in optoelectronic devices, as well as for biology and medicine. For example, the novel independent miniaturized lasers can be implanted into the cornea, skin, and whole blood, thus opening the way for long-term diagnostics and sensor data acquisition. Knowingly used LCs might lead to the development of defined size resonators in the form of droplets. Nowadays, it is possible to create a device with a strong beam power and small size (range of micrometers). Also, the size of droplets, their number, and the type of their distribution can be easily controlled at the fabrication stage. Moreover, various and straightforward methods (homogenization in the ultrasonic water bath or use of a vortex) can be further investigated. The disordered character of PDLCs might create the basis for obtaining a low lasing threshold. The change of droplet size can give the possibility to achieve band-edge lasing even in the same system [193]. The simple change between obtained effects can provide the creation of low-cost laser sources for various applications. In the case of lasing from a droplet cavity, it is worth recalling the WGM mechanism, characterized by a high *Q* factor. The construction and small size of these lasers are mainly dedicated to soft-matter-based bio- or chemosensors and miniaturized lasers [158]. Many efforts now are put to identify materials compatible with the lasers to optimize a fully wireless data transmission technology (Li-Fi technology). For this purpose, many sources of white light are in demand. Therefore, microresonators formed by LC mesophase are good candidates for creating two and three colors emitting systems, also leading to white lasing.

The applications of LC-based lasers are highly diverse, including novel data delivering and lighting technologies (like Li-Fi), sensing and biosensing, and display technologies. It is difficult to assess how much the lasers will have to be miniaturized, adapted, simplified, or maybe complicated in terms of future necessity. It is already known that LCs in the past were heavily exploited as LCDs, and this technology has already been replaced by much more effective solutions, such as LED or OLED. However, it should be remembered that the properties of LCs remain uncommonly valuable and are still not fully understood.

Author contributions: All the authors have accepted responsibility for the entire content of this submitted manuscript and approved submission.
Research funding: J.M. acknowledges the support of The National Science Center, Poland (2018/31/B/ST8/02832).
Conflict of interest statement: The authors declare no conflicts of interest regarding this article.

Appendix

AIE	Aggregation-induced-emission
ASE	Amplified spontaneous emission
BP	Blue phase
BR	Bragg reflector
ChLC	Cholesteric phase
ChLCL	Cholesteric liquid crystal lasers
CLC	Cholesteric liquid crystal
CLCE	Cholesteric liquid crystal elastomer
CMOS	Complementary metal-oxide semiconductor
CW	Continuous wave
DBR	Distributed Bragg reflector
DDBP	Dye-doped blue phase
DDChLC	Dye-doped cholesteric liquid crystal
DDLC	Dye-doped LC
DDNLC	Dye-doped nematic LC
DDPDLC	Dye-doped polymer-dispersed liquid crystal
DFB	Distributed feedback
DTCs	Double-twist cylinders
FETs	Field-effect transistors
FB	Fabry Perot
HM	Heavy metals
HPDLC	Holographic polymer dispersed liquid crystal
Iso	Isotropic
LASER	Light amplification by stimulated emission of radiation
LC	Liquid crystal
LCD	Liquid crystal displays
LSPR	Localized surface plasmon resonance
N-DDPDLC	Nonoriented dye-doped polymer-dispersed liquid crystals
NLC	Nematic liquid crystal
NLO	Nonlinear optical
NPs	Nanoparticles
oLEDs	Organic light-emitting diodes
OPA	Optical parametric amplifiers
OPO	Optical parametric oscillators
PBG	Photonic bandgap
PDLC	Polymer dispersed liquid crystal
P-DDPDLC	Oriented dye-doped polymer-dispersed liquid crystals
PSBP	Polymer-stabilized blue phase
PSChLCs	Polymer-stabilized cholesteric liquid crystals
QD	Quantum dot
QD-ChLC	Quantum dot-cholesteric liquid crystal
QD – PDLCs	Quandum dots – polymer dispersed liquid crystals
RC	Random cavity
RGB	Red green blue
RH	Real humidity
SE	Spontaneous emission
Sm	Smectic
SPs	Surface plasmons
SPR	Surface plasmon resonance
STE	Stimulated emision
TBC	Two beam coupling
UCNPs	Up-conversion nanoparticles
WHO	World health organization
WGM	Whispering gallery mode
VCSEL	Vertical cavity surface emitting laser

References

[1] L. S. Goldberg and J. Schnur, "Tunable internal-feedback liquid crystal-dye laser," U.S. Patent 3 771 065, 1973.

[2] V. I. Kopp, B. Fan, H. K. M. Vithana, and A. Z. Genack, "Low-threshold lasing at the edge of a photonic stop band in cholesteric liquid crystals," *Opt. Lett.*, vol. 23, p. 1707, 1998.

[3] V. I. Kopp, Z.-Q. Zhang, and A. Z. Genack, "Lasing in chiral photonic structures," *Prog. Quant. Electron.*, vol. 27, pp. 369–416, 2003.

[4] A. D. Ford, S. M. Morris, and H. J. Coles, "Photonics and lasing in liquid crystals," *Mater. Today*, vol. 9, pp. 36–42, 2006.

[5] A. Muñoz, Palffy-Muhoray, and B. Taheri, "Ultraviolet lasing in cholesteric liquid crystals," *Opt. Lett.*, vol. 26, pp. 804–806, 2001.

[6] C. Wenyi, A. Muñoz, P. Palffy-Muhoray, and B. Taheri, "Lasing in a three-dimensional photonic crystal of the liquid crystal blue phase II," *Nat. Mater.*, vol. 1, pp. 111–113, 2002.

[7] H. Finkelmann, S. T. Kim, A. Muñoz, P. Palffy-Muhoray, and B. Taheri, "Tunable mirrorless lasing in cholesteric liquid crystalline elastomers," *Adv. Mater.*, vol. 13, no. 14, p. 18, 2001.

[8] M. Ozaki, M. Kasano, D. Ganzke, W. Haase, and K. Yoshino, "Mirrorless lasing in a dye-doped ferrolectric liquid crystal," *Adv. Mater.*, vol. 14, pp. 306–309, 2002.

[9] A. Chanishvili, G. Chilaya, G. Petriashvili, et al., "Phototunable lasing in dye-doped cholesteric liquid crystals," *Appl. Phys. Lett.*, vol. 83, no. 26, p. 5353, 2003.

[10] R. Ozaki, T. Matsui, M. Ozaki, and K. Yoshino, "Electrically color-tunable defect mode lasing in one-dimensional photonic-band-gap system containing liquid crystal," *Appl. Phys. Lett.*, vol. 82, p. 3593, 2003.

[11] A. Chanishvili, G. Chilaya, G. Petriashvili, et al., "Lasing in dye-doped cholesteric liquid crystals: two new tuning stretegies," *Adv. Mater.*, vol. 16, pp. 9–10, 2004.

[12] S. M. Morris, A. D. Ford, M. N. Pivnenko, and H. J. Coles, "Enhanced emission from liquid-crystal lasers," *J. Appl. Phys.*, vol. 97, p. 023103, 2005.

[13] M. Ozaki, M. Kasano, T. Kitasho, D. Ganzke, W. Haase, and K. Yoshino, "Electro-tunable liquid crystal laser," *Adv. Mater.*, vol. 15, p. 12, 2003.

[14] G. Strangi, V. Barna, R. Caputo, A. De Luca, C. Cersace, and G. N. Price, "Color-tunable organic microcavity laser array using distributed feedback," *PRL*, vol. 94, p. 063903, 2005.

[15] N. Y. Ha, Y. Ohtsuka, S. M. Jeong, et al.., "Fabrication of a simultaneous red–green–blue reflector using single-pitched cholesteric liquid crystals," *Nat. Mater.*, vol. 7, 2008, https://doi.org/10.1038/nmat2045.

[16] O. Svelto, *Principles of Lasers*, New York, Springer US, 1998.

[17] R. W. Boyd, *Nonlinear Optics*, 3rd ed. Boston, MA, Academic Press, 2008.

[18] W. Demtröder, *Laser Spectroscopy 1: Basic Principles*, Berlin, Heidelberg, Springer-Verlag, 2014.

[19] I. D. W. Samuel and G. A. Turnbull, "Organic semiconductor lasers," *Chem. Rev.*, vol. 107, pp. 1272–1295, 2007.

[20] V. N. Azyazov, "Excited states in the active media of oxygen-iodine lasers," *Quant. Electron.*, vol. 39, pp. 989–1007, 2009.

[21] R. T. Schneider and F. Hohl, "Nuclear-pumped lasers," *Adv. Nucl. Sci. Technol.*, vol. 16, pp. 123–287, 1984.

[22] T. H. Maiman, "Stimulated optical radiation in Ruby," *Nature*, vol. 187, pp. 493–494, 1960.

[23] G. Cerullo and S. De Silvestri, "Ultrafast optical parametric amplifiers," *Rev. Sci. Instrum.*, vol. 74, pp. 1–18, 2003.

[24] R. Stolen and J. Bjorkholm, "Parametric amplification and frequency conversion in optical fibers," *IEEE J. Quant. Electron.*, vol. 18, pp. 1062–1072, 1982.

[25] H. J. Eichler, P. Gunter, and D. W. Pohl, *Light-induced Dynamic Gratings*, vol. 50, Berlin Heidelberg, Springer-Verlag, 1986.

[26] J. Fu, J. Zhang, T. Xue, and H. Zhao, "Large exponential gain coefficient in polymer assisted asymmetric liquid crystal cells originating from surface effect," *Opt. Commun.*, vol. 374, pp. 107–113, 2016.

[27] H. Zhao, T. Xue, H. Su, Y. Wang, and J. Zhang, "Subwavelength coupling strengthened optical amplification in nematic liquid crystal cells," *Appl. Phys. Lett.*, vol. 111, 2017, https://doi.org/10.1063/1.5003109.

[28] J. D. B. Bradley and M. Pollnau, "Erbium-doped integrated waveguide amplifiers and lasers," *Laser Photonics Rev.*, vol. 5, pp. 368–403, 2011.

[29] S. Chénais and S. Forget, "Recent advances in solid-state organic lasers," *Polym. Int.*, vol. 61, pp. 390–406, 2012.

[30] H. Kogelnik and C. V. Shank, "Coupled-wave theory of distributed feedback lasers," *J. Appl. Phys.*, vol. 43, pp. 2327–2335, 1972.

[31] L. He, Ş. K. Özdemir, and L. Yang, "Whispering gallery microcavity lasers," *Laser Photonics Rev.*, vol. 7, pp. 60–82, 2013.

[32] H. Cao, *Lasing in Random Media*, vol. 13, Waves Random Media, 2003, https://doi.org/10.1088/0959-7174/13/3/201.

[33] D. Demus, J. Goodby, G. W. Gray, H. W. Spiess, and V. Vill, *Handbook of Liquid Crystals*, Weinheim, WILEY-VCH Verlag GmbH, 1998.

[34] R. Dabrowski, P. Kula, and J. Herman, "High birefringence liquid crystals," *Crystals*, vol. 3, pp. 443–482, 2013.

[35] M. B. Ros, J. L. Serrano, M. R. De La Fuente, and C. L. Folcia, "Banana-shaped liquid crystals: A new field to explore," *J. Mater. Chem.*, vol. 15, pp. 5093–5098, 2005.

[36] A. Sobolewska, S. Bartkiewicz, J. Mysliwiec, and K. D. Singer, "Holographic memory devices based on a single-component phototropic liquid crystal," *J. Mater. Chem. C*, vol. 2, pp. 1409–1412, 2014.

[37] V. S. R. Jampani, R. H. Volpe, K. R. De Sousa, J. F. Machado, C. M. Yakacki, and J. P. F. Lagerwall, "Liquid crystal elastomer shell actuators with negative order parameter," *Sci. Adv.*, vol. 5, 2019, https://doi.org/10.1126/sciadv.aaw2476.

[38] L. Nucara, F. Greco, and V. Mattoli, "Electrically responsive photonic crystals: A review," *J. Mater. Chem. C*, vol. 3, pp. 8449–8467, 2015.

[39] H. Yoshida, K. Inoue, H. Kubo, and M. Ozaki, "Phase-dependence of gold nanoparticle dispersibility in blue phase and chiral nematic liquid crystals," *Opt. Mater. Express*, vol. 3, p. 842, 2013.

[40] Q. Guo, L. Xu, J. Sun, et al., "Fast switching beam steering based on ferroelectric liquid crystal phase shutter and polarisation grating," *Liq. Cryst.*, vol. 46, pp. 1383–1388, 2019.

[41] I. Dierking, W. Blenkhorn, E. Credland, et al., "Stabilising liquid crystalline blue phases," *Soft Matter*, vol. 8, pp. 4355–4362, 2012.

[42] E. Yablonovitch, "Photonic band-gap structures," *J. Opt. Soc. Am. B*, vol. 10, p. 283, 1993.

[43] A. Chanishvili, G. Chilaya, and G. Petriashvili, "Widely tunable ultraviolet-visible liquid crystal laser," *Appl. Phys. Lett.*, vol. 86, pp. 1–3, 2005.
[44] J. Ortega, C. L. Folcia, and J. Etxebarria, "Upgrading the performance of cholesteric liquid crystal lasers: improvement margins and limitations," *Materials*, vol. 11, 2017, https://doi.org/10.3390/ma11010005.
[45] J. Xiang, A. Varanytsia, F. Minkowski, et al., "Electrically tunable laser based on oblique heliconical cholesteric liquid crystal," *Proc. Natl. Acad. Sci. U.S.A.*, vol. 113, pp. 12925–12928, 2016.
[46] C.-W. Chen, C.-C. Li, H.-C. Jau, et al., "Electric field-driven shifting and expansion of photonic band gaps in 3D liquid photonic crystals," *ACS Photonics*, vol. 2, pp. 1524–1531, 2015.
[47] A. Varanytsia, H. Nagai, K. Urayama, and P. Palffy-Muhoray, "Tunable lasing in cholesteric liquid crystal elastomers with accurate measurements of strain," *Sci. Rep.*, vol. 5, 2015, https://doi.org/10.1038/srep17739.
[48] M. Uchimura, Y. Watanabe, F. Araoka, J. Watanabe, H. Takezoe, and G. I. Konishi, "Development of laser dyes to realize low threshold in dye-doped cholesteric liquid crystal lasers," *Adv. Mater.*, vol. 22, pp. 4473–4478, 2010.
[49] N. Wang, J. S. Evans, J. Mei, J. Zhang, I.-C. Khoo, and S. He, "Lasing properties of a cholesteric liquid crystal containing aggregation-induced-emission material," *Opt. Express*, vol. 23, p. 33938, 2015.
[50] M. Chapran, E. Angioni, N. J. Findlay, et al., "An ambipolar BODIPY derivative for a white exciplex OLED and cholesteric liquid crystal laser toward multifunctional devices," *ACS Appl. Mater. Interfaces*, vol. 9, pp. 4750–4757, 2017.
[51] L.-J. Chen, J.-D. Lin, and C.-R. Lee, "An optically stable and tunable quantum dot nanocrystal-embedded cholesteric liquid crystal composite laser," *J. Mater. Chem. C*, vol. 2, pp. 4388–4394, 2014.
[52] J.-D. Lin, M.-H. Hsieh, G.-J. Wei, T.-S. Mo, S.-Y. Huang, and C.-R. Lee, "Optically tunable/switchable omnidirectionally spherical microlaser based on a dye-doped cholesteric liquid crystal microdroplet with an azo-chiral dopant," *Opt. Express*, vol. 21, p. 15765, 2013.
[53] M. Humar and I. Muševič, "3D microlasers from self-assembled cholesteric liquid-crystal microdroplets," *Opt. Express*, vol. 18, p. 26995, 2010.
[54] Y. Iwai, R. Iijima, K. Yamamoto, T. Akita, Y. Uchida, and N. Nishiyama, "Shrinkage of cholesteric liquid crystalline microcapsule as omnidirectional cavity to suppress optical loss," *Adv. Opt. Mater.*, vol. 8, 2020, https://doi.org/10.1002/adom.201901363.
[55] L. Chen, Y. Li, J. Fan, H. K. Bisoyi, D. A. Weitz, and Q. Li, "Photoresponsive monodisperse cholesteric liquid crystalline microshells for tunable omnidirectional lasing enabled by a visible light-driven chiral molecular switch," *Adv. Opt. Mater.*, vol. 2, pp. 845–848, 2014.
[56] L.-J. Chen, L.-L. Gong, Y.-L. Lin, et al., "Microfluidic fabrication of cholesteric liquid crystal core-shell structures toward magnetically transportable microlasers," *Lab Chip*, vol. 16, pp. 1206–1213, 2016.
[57] S. S. Lee, J. B. Kim, Y. H. Kim, and S. H. Kim, "Wavelength-tunable and shape-reconfigurable photonic capsule resonators containing cholesteric liquid crystals," *Sci. Adv.*, vol. 4, 2018, https://doi.org/10.1126/sciadv.aat8276.
[58] Y. Wang, H. Li, L. Zhao, Y. Liu, S. Liu, and J. Yang, "Tunable whispering gallery modes lasing in dye-doped cholesteric liquid crystal microdroplets," *Appl. Phys. Lett.*, vol. 109, 2016, https://doi.org/10.1063/1.4971973.
[59] M. Humar, "Liquid-crystal-droplet optical microcavities," *Liq. Cryst.*, vol. 43, pp. 1937–1950, 2016.
[60] H. Lu, C. Wei, Q. Zhang, et al., "Wide tunable laser based on electrically regulated bandwidth broadening in polymer-stabilized cholesteric liquid crystal," *Photonics Res.*, vol. 7, p. 137, 2019.
[61] J.-D. Lin, H.-L. Lin, H.-Y. Lin, et al., "Widely tunable photonic bandgap and lasing emission in enantiomorphic cholesteric liquid crystal templates," *J. Mater. Chem. C*, vol. 5, pp. 3222–3228, 2017.
[62] J.-D. Lin, H.-Y. Lin, G.-J. Wei, et al., "A broadban-tunable photonic bandgap and thermally convertible laser with an ultra-low lasing threshold from a refilled chiral polymer template," *J. Mater. Chem. C*, vol. 7, pp. 4740–4747, 2019.
[63] A. Mazzulla, G. Petriashvili, M. A. Matranga, M. P. De Santo, and R. Barberi, "Thermal and electrical laser tuning in liquid crystal blue phase I," *Soft Matter*, vol. 8, pp. 4882–4885, 2012.
[64] S.-T. Hur, B. R. Lee, M.-J. Gim, K.-W. Park, M. H. Song, and S.-W. Choi, "Liquid-crystalline blue phase laser with widely tunable wavelength," *Adv. Mater.*, vol. 25, pp. 3002–3006, 2013.
[65] J.-D. Lin, S.-Y. Huang, H.-S. Wang, et al., "Spatially tunable photonic bandgap of wide spectral range and lasing emission based on a blue phase wedge cell," *Opt. Express*, vol. 22, p. 29479, 2014.
[66] H. J. Coles and M. N. Pivnenko, "Liquid crystal "blue phases" with a wide temperature range," *Nature*, vol. 436, pp. 997–1000, 2005.
[67] M. Wang, C. Zou, J. Sun, et al., "Asymmetric tunable photonic bandgaps in self-organized 3D nanostructure of polymer-stabilized blue phase I modulated by voltage polarity," *Adv. Funct. Mater.*, vol. 27, 2017. https://doi.org/10.1002/adfm.201702261.
[68] J. D. Lin, T. Y. Wang, T. S. Mo, S. Y. Huang, and C. R. Lee, "Wide-band spatially tunable photonic bandgap in visible spectral range and laser based on a polymer stabilized blue phase," *Sci. Rep.*, vol. 6, 2016, https://doi.org/10.1038/srep30407.
[69] J. Yang, J. Liu, B. Guan, et al., "Fabrication and photonic applications of large-domain blue phase films," *J. Mater. Chem. C*, vol. 7, pp. 9460–9466, 2019.
[70] G. Petriashvili, A. Chanishvili, T. Zurabishvili, et al., "Temperature tunable omnidirectional lasing in liquid crystal blue phase microspheres," *OSA Continuum*, vol. 2, p. 3337, 2019.
[71] S. S. Gandhi, Y. Li, D. Luo, and L.-C. Chien, "Laser emission in a 3D nanoporous polymer replica of amorphous blue phase III," *J. Polym. Sci, Part B: Polym. Phys.*, vol. 56, pp. 551–557, 2018.
[72] I. P. Ilchishin, L. M. Lysetskiy, T. V. Mykytiuk, and M. I. Serbina, "Reversible phototuning of lasing frequency in a dye-doped cholesteric liquid crystal," *Ukrainian J. Phys.*, vol. 56, pp. 333–338, 2011.
[73] G.-Y. Zhuo, S.-W. Huang, and S.-H. Lin, "Wide-angle lasing from photonic crystal nanostructures of a liquid-crystalline blue phase," *J. Mater. Chem. C*, vol. 7, pp. 6433–6439, 2019.
[74] S. Döring, M. Kollosche, T. Rabe, J. Stumpe, and G. Kofod, "Electrically tunable polymer DFB laser," *Adv. Mater.*, vol. 23, pp. 4265–4269, 2011.

[75] M. Ozaki, M. Kasano, T. Kitasho, D. Ganzke, W. Haase, and K. Yoshino, "Electro-tunable liquid-crystal laser," *Adv. Mater.*, vol. 15, pp. 974–977, 2003.
[76] K. Parafiniuk, L. Sznitko, and J. Mysliwiec, "Distributed feedback and random lasing in DCNP aggregates dispersed in a polymeric layer," *Opt. Lett.*, vol. 40, p. 1552, 2015.
[77] M. Stroisch, T. Woggon, C. Teiwes-Morin, et al., "Intermediate high index layer for laser mode tuning in organic semiconductor lasers," *Opt. Express*, vol. 18, p. 5890, 2010.
[78] I. P. Ilchishin and E. A. Tikhonov, "Dye-doped cholesteric lasers: distributed feedback and photonic bandgap lasing models," *Prog. Quant. Electron.*, vol. 41, pp. 1–22, 2015.
[79] W. Huang, Z. Diao, Y. Liu, et al., "Distributed feedback polymer laser with an external feedback structure fabricated by holographic polymerization technique," *Org. Electron.*, vol. 13, pp. 2307–2311, 2012.
[80] Z. Diao, W. Huang, Z. Peng, et al., "Anisotropic waveguide theory for electrically tunable distributed feedback laser from dye-doped holographic polymer dispersed liquid crystal," *Liq. Cryst.*, vol. 41, pp. 239–246, 2014.
[81] Z. Diao, L. Kong, L. Xuan, and J. Ma, "Electrical control of the distributed feedback organic semiconductor laser based on holographic polymer dispersed liquid crystal grating," *Org. Electron.*, vol. 27, pp. 101–106, 2015.
[82] W. Huang, L. Chen, and L. Xuan, "Efficient laser emission from organic semiconductor activated holographic polymer dispersed liquid crystal transmission gratings," *RSC Adv.*, vol. 4, pp. 38606–38613, 2016.
[83] K. W. Yoon and N. Y. Ha, "Electrically tunable liquid crystal laser using a nanoimprinted indium-tin-oxide electrode as a distributed feedback resonator," *Opt. Express*, vol. 24, p. 516, 2016.
[84] T. Park, S. Bae, and N. Y. Ha, "Widely tunable lasing with lowered threshold in a two-dimensional indium-tin-oxide distributed-feedback structure," *Opt. Mater. Express*, vol. 6, p. 3676, 2016.
[85] K.-Y. Yu, S.-H. Chang, C.-R. Lee, T.-Y. Hsu, and C.-T. Kuo, "Thermally tunable liquid crystal distributed feedback laser based on a polymer grating with nanogrooves fabricated by nanoimprint lithography," *Opt. Mater. Express*, vol. 4, p. 234, 2014.
[86] M. S. Li, A. Y.-G. Fuh, and S.-T. Wu, "Multimode lasing from the microcavity of an octagonal quasi-crystal based on holographic polymer-dispersed liquid crystals," *Opt. Lett.*, vol. 37, p. 3249, 2012.
[87] D. Luo, Q. G. Du, H. T. Dai, et al., "Strongly linearly polarized low threshold lasing of all organic photonic quasicrystals," *Sci. Rep.*, vol. 2, 2012. https://doi.org/10.1038/srep00627.
[88] D. Luo, Q. G. Du, H. T. Dai, X. H. Zhang, and X. W. Sun, "Temperature effect on lasing from Penrose photonic quasicrystal," *Opt. Mater. Express*, vol. 4, p. 1172, 2014.
[89] D. Luo, Y. Li, X. W. Xu, and Q. G. Du, "Lasing from organic quasicrystal fabricated by seven- and nine-beam interference," *Opt. Express*, vol. 24, p. 12330, 2016.
[90] Z. Diao, S. Deng, W. Huang, et al., "Organic dual-wavelength distributed feedback laser empowered by dye-doped holography," *J. Mater. Chem.*, vol. 22, pp. 23331–23334, 2012.
[91] O. Castany, L. Dupont, A. Shuaib, J. P. Gauthier, C. Levallois, and C. Paranthon, "Tunable semiconductor vertical-cavity surface-emitting laser with an intracavity liquid crystal layer Appl," *Phys. Lett.*, vol. 98, 2011, https://doi.org/10.1063/1.3569591.
[92] C. Levallois, B. Caillaud, J.-L. de Bougrenet de la Tocnaye, et al., "Long-wavelength vertical-cavity surface-emitting laser using an electrooptic index modulator with 10 nm tuning range," *Appl. Phys. Lett.*, vol. 89, 2006. https://doi.org/10.1063/1.2219144.
[93] C. I. Wilkinson, J. Woodhead, J. E. F. Frost, J. S. Roberts, R. Wilson, and M. F. Lewis, "Electrical polarization control of vertical-cavity surface-emitting lasers using polarized feedback and a liquid crystal," *IEEE Photonics Technol. Lett.*, vol. 11, pp. 155–157, 1999.
[94] L. Frasunkiewicz, T. Czyszanowski, H. Thienpont, and K. Panajotov, "Electrically tunable VCSEL with intra-cavity liquid crystal: design, optimization, and analysis of polarization- and mode-stability," *Opt. Commun.*, vol. 427, pp. 271–277, 2018.
[95] Y. Xie, J. Beeckman, W. Woestenborghs, K. Panajotov, and K. Neyts, "VCSEL with photo-aligned liquid crystal overlay," *IEEE Photonics Technol. Lett.*, vol. 24, pp. 1509–1512, 2012.
[96] K. Panajotov and H. Thienpont, "Vertical-cavity surface-emitting laser with liquid crystal overlay," *Opt. Express*, vol. 19, p. 16749, 2011.
[97] K. Panajotov, M. Dems, C. Belmonte, et al., "Vertical-cavity surface-emitting laser with cholesteric liquid crystal overlay," *J. Lightwave Technol.*, vol. 32, pp. 20–26, 2014.
[98] J.-D. Lin, Y.-S. Zhang, J.-Y. Lee, T.-S. Mo, H.-C. Yeh, and C.-R. Lee, "Electrically tunable liquid-crystal-polymer composite laser with symmetric sandwich structure," *Macromolecules*, vol. 53, pp. 913–921, 2020.
[99] B. Boisnard, C. Levallois, C. Paranthoen, et al., "CW operation of a tunable 1550-nm VCSEL integrating liquid-crystal microcells," *IEEE Photonics Technol. Lett.*, vol. 32, pp. 391–394, 2020.
[100] S. E. Skipetrov, "Disorder is the new order," *Nature*, vol. 432, pp. 285–286, 2004.
[101] S. Ferjani, V. Barna, A. De Luca, et al., "Thermal behavior of random lasing in dye doped nematic liquid crystals," *Appl. Phys. Lett.*, vol. 89, 2006. https://doi.org/10.1063/1.2356087.
[102] Q. Song, S. Xiao, X. Zhou, et al., "Liquid crystals based tunable high-Q directional random laser from a planar random microcavity," in *Optics InfoBase Conference Papers*, vol. 32, 2007, pp. 373–375.
[103] A. Adamow, A. Szukalski, L. Sznitko, et al., "Electrically controlled white laser emission through liquid crystal/polymer multiphases," *Light Sci. Appl.*, vol. 9, 2020. https://doi.org/10.1038/s41377-020-0252-9.
[104] P. Palffy-Muhoray, W. Cao, M. Moreira, B. Taheri, and A. Munoz, "Photonics and lasing in liquid crystal materials," *Phil. Trans. R. Soc. A Math. Phys. Eng. Sci.*, vol. 364, pp. 2747–2761, 2006.
[105] Q. Song, L. Liu, L. Xu, Y. Wu, and Z. Wang, "Electrical tunable random laser emission from a liquid-crystal infiltrated disordered planar microcavity," *Opt. Lett.*, vol. 34, p. 298, 2009.
[106] H. T. Dai, M. N. Gao, Y. X. Xue, et al., "Magnetically tunable random lasing from polymer dispersed liquid crystal doped ferromagnetic nanoparticles in capillary," *AIP Adv.*, vol. 9, 2019. https://doi.org/10.1063/1.5120438.
[107] G. Strangi, S. Ferjani, V. Barna, et al., "Random lasing and weak localization of light in dye-doped nematic liquid crystals," *Opt. Express*, vol. 14, p. 7737, 2006.
[108] F. Yao, H. Bian, Y. Pei, C. Hou, and X. Sun, "Behaviors of random laser in dye-doped nematic liquid crystals," *Opt. Commun.*, vol. 359, pp. 15–19, 2016.

[109] W. Cao, A. Muñoz, P. Palffy-Muhoray, and B. Taheri, "Lasing in a three-dimensional photonic crystal of the liquid crystal blue phase II," *Nat. Mater.*, vol. 1, pp. 111–113, 2002.
[110] J. Schmidtke, W. Stille, H. Finkelmann, and S. T. Kim, "Laser emission in a dye doped cholesteric polymer network," *Adv. Mater.*, vol. 14, pp. 746–749, 2002.
[111] H. Cao, J. Y. Xu, E. W. Seelig, and R. P. H. Chang, "Microlaser made of disordered media," *Appl. Phys. Lett.*, vol. 76, pp. 2997–2999, 2000.
[112] H. Bian, F. Yao, H. Liu, et al., "Optically controlled random lasing based on photothermal effect in dye-doped nematic liquid crystals," *Liq. Cryst.*, vol. 41, pp. 1436–1441, 2014.
[113] C. R. Lee, J. D. Lin, B. Y. Huang, et al., "Electrically controllable liquid crystal random lasers below the Fréedericksz transition threshold," *Opt. Express*, vol. 19, p. 239, 2011.
[114] F. Yao, W. Zhou, H. Bian, et al., "Polarization and polarization control of random lasers from dye-doped nematic liquid crystals," *Opt. Lett.*, vol. 38, p. 1557, 2013.
[115] J. L. Zhu, W. H. Li, Y. Sun, et al., "Random laser emission in a sphere-phase liquid crystal," *Appl. Phys. Lett.*, vol. 106, 2015. https://doi.org/10.1063/1.4921325.
[116] J. L. Zhu, S. B. Ni, C. P. Chen, et al., "Chiral-induced self-assembly sphere phase liquid crystal with fast switching time," *Appl. Phys. Lett.*, vol. 104, 2014. https://doi.org/10.1063/1.4867358.
[117] R. Wu, J. Lu, X. Wang, F. Yang, Y. Li, and Q. Dai, "Random lasing in dye-doped chiral nematic liquid crystal," *Optik*, vol. 202, p. 163616, 2020.
[118] D. S. Wiersma, "The physics and applications of random lasers," *Nat. Phys.*, vol. 4, pp. 359–367, 2008.
[119] L. M. Blinov, G. Cipparrone, P. Pagliusi, V. V. Lazarev, and S. P. Palto, "Mirrorless lasing from nematic liquid crystals in the plane waveguide geometry without refractive index or gain modulation," *Appl. Phys. Lett.*, vol. 89, 2006, https://doi.org/10.1063/1.2234316.
[120] Y. G. Marinov, G. B. Hadjichristov, A. G. Petrov, S. Marino, C. Versace, and N. Scaramuzza, "Electro-optical response of polymer-dispersed liquid crystal single layers of large nematic droplets oriented by rubbed teflon nanolayers," *J. Appl. Phys.*, vol. 113, 2013, https://doi.org/10.1063/1.4789897.
[121] S. Bronnikov, S. Kostromin, and V. Zuev, "Polymer-dispersed liquid crystals: progress in preparation, investigation, and application," *J. Macromol. Sci. Part B Phys.*, vol. 52, pp. 1718–1735, 2013.
[122] G. De Filpo, P. Formoso, S. Manfredi, A. I. Mashin, and F. P. Nicoletta, "Preparation and characterisation of bifunctional reverse-mode polymer-dispersed liquid crystals," *Liq. Cryst.*, vol. 44, pp. 1607–1616, 2017.
[123] S. Zumer, "Light scattering from nematic droplets: anomalous-diffraction approach," *Phys. Rev. A*, vol. 37, pp. 4006–4015, 1988.
[124] T. Gotoh and H. Murai, "Preparation and characteristics of new reverse mode film of polymer dispersed liquid crystal type," *Appl. Phys. Lett.*, vol. 60, pp. 392–394, 1992.
[125] S. Gottardo, S. Cavalieri, O. Yaroshchuk, and D. S. Wiersma, "Quasi-two-dimensional diffusive random laser action," *Phys. Rev. Lett.*, vol. 93, 2004, https://doi.org/10.1103/physrevlett.93.263901.
[126] Y. J. Liu, X. W. Sun, H. I. Elim, and W. Ji, "Gain narrowing and random lasing from dye-doped polymer-dispersed liquid crystals with nanoscale liquid crystal droplets," *Appl. Phys. Lett.*, vol. 89, 2006, https://doi.org/10.1063/1.2219988.
[127] L. Ye, C. Lv, F. Li, Y. Wang, B. Liu, and Y. Cui, "Effect of alignment layer on polymer-dispersed liquid crystal random laser," *J. Mod. Opt.*, vol. 64, pp. 1429–1434, 2017.
[128] R. C. Polson and Z. V. Vardeny, "Random lasing in human tissues Appl," *Phys. Lett.*, vol. 85, pp. 1289–1291, 2004.
[129] Z. Shang, M. Yang, and L. Deng, "Low-threshold and high intensity random lasing enhanced by MnCl2," *Materials*, vol. 9, 2016, https://doi.org/10.3390/ma9090725.
[130] L. Li and L. Deng, "Random lasers in dye-doped polymer-dispersed liquid crystals containing silver nanoparticles," *Phys. B Condens. Matter*, vol. 407, pp. 4826–4830, 2012.
[131] L. Li, L. Wang, and L. Deng, "Low threshold random lasing in DDPDLCs, DDPDLC@ZnO nanoparticles and dye solution@ZnO nanoparticle capillaries," *Laser Phys. Lett.*, vol. 11, 2014, https://doi.org/10.1088/1612-2011/11/2/025201.
[132] J.-H. Lin, and Y.-L. Hsiao, "Manipulation of the resonance characteristics of random lasers from dye-doped polymer dispersed liquid crystals in capillary tubes," *Opt. Mater. Express*, vol. 4, p. 1555, 2014.
[133] T. H. Dai, M. N. Gao, Y. X. Xue, et al., "Magnetically tunable random lasing from polymer dispersed liquid crystal doped ferromagnetic nanoparticles in capillary," *AIP Adv.*, vol. 9, p. 115015, 2019.
[134] L. Ye, B. Liu, F. Li, Y. Feng, Y. Cui, and Y. Lu, "The influence of Ag nanoparticles on random laser from dye-doped nematic liquid crystals," *Laser Phys. Lett.*, vol. 13, 2016, https://doi.org/10.1088/1612-2011/13/10/105001.
[135] H. Raether, G. Hohler, and E. A. Niekisch, "Surface plasmons on smooth and rough surfaces and on gratings," *Springer Tr. Mod. Phys.*, vol. 111, p. 136, 1988.
[136] Y. Wan, Y. An, and L. Deng, "Plasmonic enhanced low-threshold random lasing from dye-doped nematic liquid crystals with TiN nanoparticles in capillary tubes," *Sci. Rep.*, vol. 7, 2017, https://doi.org/10.1038/s41598-017-16359-5.
[137] C.-R. Lee, S.-H. Lin, C.-H. Guo, S.-H. Chang, T.-S. Mo, and S.-C. Chu, "All-optically controllable random laser based on a dye-doped polymer-dispersed liquid crystal with nano-sized droplets," *Opt. Express*, vol. 18, p. 2406, 2010.
[138] D. S. Wiersma, M. Colocci, R. Righini, and F. Aliev, "Temperature-controlled light diffusion in random media," *Phys. Rev. B Condens. Matter*, vol. 64, pp. 1442081–1442086, 2001.
[139] M. Cao, "Enhanced amplified spontaneous emission in a quantum dot-doped polymer-dispersed liquid crystal," *Nanotechnology*, vol. 27, 2016, https://doi.org/10.1088/0957-4484/27/26/26lt01.
[140] L. W. Li, Z. Z. Shang, and L. Deng, "Random lasing from dye-doped negative liquid crystals using ZnO nanoparticles as tunable scatters," *Chin. Phys. B*, vol. 25, 2016, https://doi.org/10.1088/1674-1056/25/9/090301.
[141] L. Li, "Random lasers tuning by combining a dye-doped liquid crystal and CdS nanoparticles," *Optik*, vol. 134, pp. 1–8, 2017.
[142] Z. Wang, M. Cao, G. Shao, et al., "Coherent random lasing in colloidal quantum dot-doped polymer-dispersed liquid crystal with low threshold and high stability," *J. Phys. Chem. Lett.*, vol. 11, pp. 767–774, 2020.
[143] S. A. Veldhuis, P. P. Boix, N. Yantara, et al., "Perovskite materials for light-emitting diodes and lasers," *Adv. Mater.*, vol. 28, pp. 6804–6834, 2016.

[144] S. D. Stranks, S. M. Wood, K. Wojciechowski, et al., "Enhanced amplified spontaneous emission in perovskites using a flexible cholesteric liquid crystal reflector," *Nano Lett.*, vol. 15, pp. 4935–4, 2015.
[145] V. D'Innocenzo, G. Grancini, M. J. P. Alcocer, et al., "Excitons versus free charges in organo-lead tri-halide perovskites," *Nat. Commun.*, vol. 5, 2014.
[146] S. M. Jeong, K. Sonoyama, Y. Takanishi, et al., "Optical cavity with a double-layered cholesteric liquid crystal mirror and its prospective application to solid state laser," *Appl. Phys. Lett.*, vol. 89, 2006. https://doi.org/10.1063/1.2404937.
[147] Q. Lin, A. Armin, R. C. R. Nagiri, P. L. Burn, and P. Meredith, "Electro-optics of perovskite solar cells," *Nat. Photonics*, vol. 9, pp. 106–112, 2015.
[148] G. Xing, N. Mathews, S. S. Lim, et al., "Low-temperature solution-processed wavelength-tunable perovskites for lasing," *Nat. Mater.*, vol. 13, pp. 476–480, 2014.
[149] F. Deschler, M. Price, S. Pathak, et al., "High photoluminescence efficiency and optically pumped lasing in solution-processed mixed halide perovskite semiconductors," *J. Phys. Chem. Lett.*, vol. 5, pp. 1421–1426, 2014.
[150] W. Sun, K. Wang, Z. Gu, S. Xiao, and Q. Song, "Tunable perovskite microdisk lasers," *Nanoscale*, vol. 8, pp. 8717–8721, 2016.
[151] L.-J. Chen, J.-H. Dai, J.-D. Lin, et al., "Wavelength-tunable and highly stable perovskite-quantum-dot-doped lasers with liquid crystal lasing cavities," *ACS Appl. Mater. Interfaces*, vol. 10, pp. 33307–33315, 2018.
[152] G. M. Arumugam, C. Xu, S. K. Karunakaran, et al., "Low threshold lasing from novel thulium-incorporated C(NH2)3PbI3 perovskite thin films in Fabry-Pérot resonator," *J. Mater. Chem. C*, vol. 6, pp. 12537–12546, 2018.
[153] G. E. Nevskaya, S. P. Palto, and M. G. Tomilin, "Liquid-crystal-based microlasers," *J. Opt. Technol.*, vol. 77, p. 473, 2010.
[154] A. Chiasera, Y. Dumeige, P. Féron, et al., "Spherical whispering-gallery-mode microresonators," *Laser Photonics Rev.*, vol. 4, pp. 457–482, 2010.
[155] I. S. Grudinin, V. S. Ilchenko, and L. Maleki, "Ultrahigh optical Q factors of crystalline resonators in the linear regime," *Phys. Rev. A – At. Mol. Opt. Phys.*, vol. 74, 2006, https://doi.org/10.1103/physreva.74.063806.
[156] C. Yang, H. Zhang, B. Liu, S. Lin, Y. Li, and H. Liu, "Electrically tunable whispering gallery mode microresonator based on a grapefruit-microstructured optical fiber infiltrated with nematic liquid crystals," *Opt. Lett.*, vol. 42, p. 2988, 2017.
[157] L. Zhao, Y. Wang, Y. Yuan, et al., "Whispering gallery mode laser based on cholesteric liquid crystal microdroplets as temperature sensor," *Opt. Commun.*, vol. 402, pp. 181–185, 2017.
[158] A. Mahmood, V. Kavungal, S. S. Ahmed, et al., "Magnetic field sensing using whispering-gallery modes in a cylindrical microresonator infiltrated with ferronematic liquid crystal," *Opt. Express*, vol. 25, p. 12195, 2017.
[159] M. Mur, J. A. Sofi, I. Kvasić, et al., "Magnetic-field tuning of whispering gallery mode lasing from ferromagnetic nematic liquid crystal microdroplets," *Opt. Express*, vol. 25, p. 1073, 2017.
[160] A. Adamow, L. Sznitko, and J. Mysliwiec, "The influence of homogenization process on lasing performance in polymer-nematic liquid crystal emulsions," *Opt. Mater.*, vol. 69, pp. 81–86, 2017.
[161] R. F. Oulton, V. J. Sorger, T. Zentgraf, et al., "Plasmon lasers at deep subwavelength scale," *Nature*, vol. 461, pp. 629–632, 2009.
[162] H. C. Cheng, C. Y. Kuo, Y. J. Hung, K. P. Chen, and S. C. Jeng, "Liquid-crystal active tamm-plasmon devices," *Phys. Rev. Appl.*, vol. 9, 2018, https://doi.org/10.1103/physrevapplied.9.064034.
[163] Y. S. Liu, H. C. Lin, and H. L. Xu, "The surface plasmon resonance effect on the defect-mode cholesteric liquid crystals doped with gold nanoparticles," *IEEE Photonics J.*, vol. 10, 2018, https://doi.org/10.1109/jphot.2018.2821560.
[164] J. Olson, A. Manjavacas, T. Basu, et al., "High chromaticity aluminum plasmonic pixels for active liquid crystal displays," *ACS Nano*, vol. 10, pp. 1108–1117, 2016.
[165] K. Tiwari, A. K. Singh, and S. C. Sharma, "Evidence for surface plasmons in a liquid crystal containing gold nanoparticles," *Appl. Phys. Lett.*, vol. 101, 2012, https://doi.org/10.1063/1.4772066.
[166] S. Y. Park and D. Stroud, "Splitting of surface plasmon frequencies of metal particles in a nematic liquid crystal," *Appl. Phys. Lett.*, vol. 85, pp. 2920–2922, 2004.
[167] C. T. Chen, C. C. Liu, C. H. Wang, C. W. Chen, and Y. F. Chen, "Tunable coupling between exciton and surface plasmon in liquid crystal devices consisting of Au nanoparticles and CdSe quantum dots," *Appl. Phys. Lett.*, vol. 98, 2011, https://doi.org/10.1063/1.3606539.
[168] Y. Yamamoto and R. E. Slusher, "Optical processes in microcavities," *Phys. Today*, vol. 46, pp. 66–73, 1993.
[169] C.-H. Chen and K.-L. Yang, "A liquid crystal biosensor for detecting organophosphates through the localized pH changes induced by their hydrolytic products," *Sensor. Actuator. B Chem.*, vol. 181, pp. 368–374, 2013.
[170] D.-Y. Lee, J.-M. Seo, W. Khan, J. A. Kornfield, Z. Kurji, and S.-Y. Park, "PH-responsive aqueous/LC interfaces using SGLCP-b-polyacrylic acid block copolymers," *Soft Matter*, vol. 6, pp. 1964–1970, 2010.
[171] J.-M. Seo, W. Khan, and S.-Y. Park, "Protein detection using aqueous/LC interfaces decorated with a novel polyacrylic acid block liquid crystalline polymer," *Soft Matter*, vol. 8, pp. 198–203, 2012.
[172] Y. Wang, L. Zhao, A. Xu, et al., "Detecting enzymatic reactions in penicillinase via liquid crystal microdroplet-based pH sensor," *Sensor. Actuator. B Chem.*, vol. 258, pp. 1090–1098, 2018.
[173] Z. Wang, Y. Zhang, X. Gong, et al., "Bio-electrostatic sensitive droplet lasers for molecular detection," *Nanoscale Adv.*, vol. 2, pp. 2713–2719, 2020.
[174] R. Duan, Y. Li, H. Li, and J. Yang, "Detection of heavy metal ions using whispering gallery mode lasing in functionalized liquid crystal microdroplets," *Biomed. Opt. Express*, vol. 10, p. 6073, 2019.
[175] R. Duan, Y. Li, B. Shi, H. Li, and J. Yang, "Real-time, quantitative and sensitive detection of urea by whispering gallery mode lasing in liquid crystal microdroplet," *Talanta*, vol. 209, 2020, https://doi.org/10.1016/j.talanta.2019.120513.
[176] P. K. Mukherjee, "Theory of biomolecular interactions at phospholipid-decorated surfaces of liquid crystals," *J. Mol. Liq.*, vol. 199, pp. 133–136, 2014.

[177] S. Zhong and C.-H. Jang, "Highly sensitive and selective glucose sensor based on ultraviolet-treated nematic liquid crystals," *Biosens. Bioelectron.*, vol. 59, pp. 293–299, 2014.
[178] V. K. Gupta, J. J. Skaife, T. B. Dubrovsky, and N. L. Abbott, "Optical amplification of ligand-receptor binding using liquid crystals," *Science*, vol. 80, no. 279, pp. 2077–2080, 1998.
[179] M. I. Kinsinger, B. Sun, N. L. Abbott, and D. M. Lynn, "Reversible control of ordering transitions at aqueous/liquid crystal interfaces using functional amphiphilic polymers," *Adv. Mater.*, vol. 19, pp. 4208–4212, 2007.
[180] C.-H. Chen, Y.-C. Lin, H.-H. Chang, and A. S.-Y. Lee, "Ligand-doped liquid crystal sensor system for detecting mercuric ion in aqueous solutions," *Anal. Chem.*, vol. 87, pp. 4546–4551, 2015.
[181] S. Hu, S. Wu, C. Li, R. Chen, E. Forsberg, and S. He, "SNR-enhanced temperature-insensitive microfiber humidity sensor based on upconversion nanoparticles and cellulose liquid crystal coating," *Sensor. Actuator. B Chem.*, vol. 305, p. 127517, 2020.
[182] L. Ye, C. Zhao, Y. Feng, B. Gu, Y. Cui, and Y. Lu, "Study on the polarization of random lasers from dye-doped nematic liquid crystals," *Nanoscale Res. Lett.*, vol. 12, 2017, https://doi.org/10.1186/s11671-016-1778-x.
[183] F. F. Xu, Y. J. Li, Y. Lv, et al., "Flat-panel laser displays based on liquid crystal microlaser arrays," *CCS Chem.*, vol. 2, pp. 369–375, 2020.
[184] M. Humar, M. Ravnik, S. Pajk, and I. Muševič, "Electrically tunable liquid crystal optical microresonators," *Nat. Photonics*, vol. 3, pp. 595–600, 2009.
[185] M. Sutkowski, T. Grudniewski, J. Parka, and A. Miniewicz, "Holographic movies projected onto nematic LC cells. XIV Conference on Liquid Crystals," *Chem. Phys. Appl.*, vol. 4759, p. 445, 2002.
[186] D. S. Wiersma and S. Cavalieri, "Light emission: A temperature-tunable random laser," *Nature*, vol. 414, pp. 708–709, 2001.
[187] A. Miniewicz, A. Samoc, M. Samoc, and P. Kaszynski, "Observation of second-harmonic generation in an oriented glassy nematic phase of a closo-decaborane derivative," *J. Appl. Phys.*, vol. 200, p. 102, 2007.
[188] S. Perumbilavil, A. Piccardi, O. Buchnev, M. Kauranen, G. Strangi, and G. Assanto, "All-optical guided-wave random laser in nematic liquid crystals," *Opt. Express*, vol. 25, p. 4672, 2017.
[189] J. Justice, C. Bower, M. Meitl, M. B. Mooney, M. A. Gubbins, and B. Corbett, "Wafer-scale integration of group III-V lasers on silicon using transfer printing of epitaxial layers Nat," *Photonics*, vol. 6, pp. 610–614, 2012.
[190] G. Ulrich, R. Ziessel, and A. Harriman, "The chemistry of fluorescent bodipy dyes: versatility unsurpassed," *Angew. Chem. Int. Ed.*, vol. 47, pp. 1184–1201, 2008.
[191] M. A. Rahman, S. Mohd Said, and S. Balamurugan, "Blue phase liquid crystal: strategies for phase stabilization and device development," *Sci. Technol. Adv. Mater.*, vol. 16, 2015, https://doi.org/10.1088/1468-6996/16/3/033501.
[192] W. Huang, D. Pu, W. Qiao, et al., "Tunable multi-wavelength polymer laser based on a triangular-lattice photonic crystal structure," *J. Phys. D. Appl. Phys.*, vol. 49, 2016. https://doi.org/10.1088/0022-3727/49/33/335103.
[193] P. J. W. Hands, D. J. Gardiner, S. M. Morris, C. Mowatt, T. D. Wilkinson, and H. J. Coles, "Band-edge and random lasing in paintable liquid crystal emulsions," *Appl. Phys. Lett.*, vol. 98, 2011, https://doi.org/10.1063/1.3574915.